

1 **Developing a tile drainage module for Cold Regions**  
2 **Hydrological Model: Lessons from a farm in Southern**  
3 **Ontario, Canada**

4

5 Mazda Kompanizare<sup>\*&#</sup>, Diogo Costa<sup>+</sup>, Merrin L. Macrae<sup>&</sup>, John W. Pomeroy<sup>\*</sup>, Richard M. Petrone<sup>&</sup>

6 <sup>\*</sup>Centre for Hydrology, University of Saskatchewan, Canmore and Saskatoon, Canada

7 <sup>+</sup>University of Évora, Mediterranean Institute for Agriculture, Environment and Development, Portugal

8 <sup>&</sup>University of Waterloo, Waterloo, Canada

9 <sup>#</sup>Corresponding author: kompanizare.mazda@usask.ca

10

11 **Abstract**

12 Systematic tile drainage is used extensively in agricultural lands to remove excess water and  
13 improve crop growth; however, tiles can also transfer nutrients from farmlands to downstream  
14 surface water bodies, leading to water quality problems. Thus, there is a need to simulate the  
15 hydrological behaviour of tile drains to understand the impacts of climate or land management  
16 change on agricultural runoff. The Cold Regions Hydrological Model (CRHM) is a physically  
17 based, modular modeling system developed for cold regions. Here, a tile drainage module is  
18 developed for CRHM. A multi-variable, multi-criteria model performance evaluation strategy  
19 was deployed to examine the ability of the module to capture tile discharge under both winter  
20 and summer conditions (NSE>0.29, RSR<0.84 and PBias <20 for tile flow and water table  
21 simulations). Initial model -simulations run at a 15-min interval did not satisfactorily represent

22 tile discharge; however, model simulations improved when the time step was ~~lengthened~~refined  
23 to hourly but also with the explicit representation of capillary rise for moisture interactions  
24 between the rooting zone and groundwater, demonstrating the significance of capillary rise  
25 above the water table in the hydrology of tile drains in loam soils. Novel aspects of this module  
26 include the sub-daily ~~shorter time step~~time step, which is shorter than most ~~relative to some~~  
27 existing models, and which may enable future water quality modules to be added, and the use of  
28 field capacity and its corresponding pressure head to provide estimates of drainable water and the  
29 thickness of the capillary fringe, rather using than detailed soil retention curves that may not  
30 always be available. An additional novel aspect ~~of our results~~ is the demonstration that flows in  
31 some tile drain systems can be better represented and simulated when related to shallow water  
32 table groundwater dynamics.

33

34 Keywords: tile drainage, cold regions, hydrological model, capillary fringe, drainable water,  
35 water table~~level~~ fluctuations

36

37

## 38 **1. Introduction**

39

40 Harmful algal blooms and eutrophication in large freshwater lakes surrounded by agricultural  
41 lands are major environmental challenges in Canada and globally. The transport of nutrients,  
42 particularly phosphorus, in runoff from agricultural fields into rivers, ponds and eventually lakes  
43 is an important contributor to the increased frequency of algal blooms being experienced in  
44 North America and elsewhere (Sharpley et al., 1995; Correll, 1998; Filippelli, 2002; Ruttenberg,

45 2005; Schindler, 2006; Quinton et al., 2010; Costa et al., 2022). Nutrient transport from  
46 agricultural fields can occur via both surface runoff and tile drainage (Radcliffe et al., 2015), and  
47 recent increases in the frequency and magnitude of algal blooms in Lake Erie in North America  
48 have been attributed to tile drainage (King et al., 2015; Jarvie et al., 2017). Tile drain systems  
49 reduce the retention time of soil water, lessening waterlogging in fields and improving both crop  
50 growth and field trafficability for farmers (Cordeiro and Ranjan, 2012; Kokulan et al., 2019a).  
51 However, they are also important pathways for dissolved and particulate nutrients (Kladivko et  
52 al., 1999; Tomer et al., 2015). It has been estimated that 14% of farmlands in Canada (ICID,  
53 2018) and 45% of fields in Southern Ontario, Canada (ICID, 2018; Kokulan, 2019) are drained  
54 by tile systems. In Alberta, tile drains have also been used to address salinity issues (Broughton  
55 and Jutras, 2013). Given their importance in hydrological budgets and biogeochemical transport,  
56 there is a need to understand the controlling mechanisms of water and nutrient export from tile  
57 systems as an integral part of the broader, modified hydrological system. The ability to integrate  
58 a dynamic quantification of tile drainage from fields in hydrological models can help understand  
59 the relative importance of this human-induced process as it interplays with an array of other  
60 phenomena, including energy and physical mass balance hydrological processes, climate change,  
61 and the impacts of modified land management practices on runoff and nutrient export.

62         There are several models that can represent tile drainage at the small basin scale, such as  
63 HYPE (Lindstrom et al., 2010; Arheimer et al., 2015), DRAINMOD (Skaggs, 1978, 1980a;  
64 Skaggs et al., 2012), MIKE SHE (Refsgaard and Storm, 1995) and SWAT (Arnold et al., 1998;  
65 Koch et al., 2013; Du et al., 2005; Du et al., 2006; Green et al., 2006; Kiesel et al., 2010). These  
66 models include conceptual components for many key hydrological processes, but research shows  
67 that they have been primarily designed and tested for temperate regions (Costa et al., 2020a). In

68 Canada and other cold regions, some unique hydrological processes such as frozen soil,  
69 snowmelt, rain on snow, and runoff over and infiltration into frozen or partially-frozen soils may  
70 be very important (Rahman et al., 2014; Cordeiro et al., 2017; Pomeroy et al., 1998, 2007; Fang  
71 et al., 2010, 2013). Many hydrological processes, such as the sublimation of snow, energy  
72 balance snowmelt, and infiltration into frozen soils, are strongly affected by temperature and the  
73 phase changes of water, which make many existing models developed for warm regions less  
74 appropriate for regions with cold seasons (Pomeroy et al., 2007; Pomeroy et al., 2013; Pomeroy  
75 et al., 2016; Fang et al., 2010, 2013). Even for temperate regions, the representation of cold  
76 season processes is often underrepresented in models (Costa et al., 2020a).

77         Since the use of tile drainage is becoming popular in many cold regions, it has become  
78 important to integrate such human-induced process in specialized hydrological modelling tools  
79 for these regions, such as the Cold Regions Hydrological Modelling platform (CRHM, Pomeroy  
80 et al., 2007; 2013; 2022). CRHM was initially developed in 1998 to assemble and explore the  
81 hydrological understanding developed from a series of research basins spanning Canada and  
82 elsewhere into a flexible, modular, object-oriented, multiphysics platform for simulating  
83 hydrological processes and basin response in cold regions (Pomeroy et al., 2007; 2022). The  
84 modular CRHM platform allows for multiple representations of forcing data interpolation and  
85 extrapolation, hydrological model spatial and physical process structure and parameter values.  
86 Many existing models typically operate at default daily or monthly time intervals, which is  
87 inadequate for the prediction of many short-duration “flashy” hydraulic responses often observed  
88 in tiles (Pluer et al., 2020; Vivekananthan, 2019; Vivekananthan et al., 2019; Lam et al., 2016a,  
89 2016b; Macrae et al., 2019). Indeed, the ability to simulate shorter time intervals (e.g., hourly)  
90 facilitates the ability to capture both the rising and falling limbs of tile flow hydrographs, as well

91 as the magnitude of peak flows, both of which are important to tile drain chemistry and export  
92 (Rozemeijer et al., 2016; Williams et al., 2015, 2016; Macrae et al., 2019).

93 Hydrological process models such as DRAINMOD, MIKE SHE and SWAT use a  
94 combination of empirical and physically based formulations for the simulation of tile flow  
95 derived by Hooghoudt (1940), Kirkham (1957), van Schilfgaarde (1974), Bouwer and van  
96 Schilfgaarde (1963) and Skaggs et al., (1978). Such formulations contemplate both cases where  
97 the water table is below and above the ground surface (Kirkham, 1957). In contrast, simulations  
98 of tile drainage in other models such as HYPE use empirically derived recession curves  
99 (Eckersten et al., 1994) to simulate tile flow and soil hydrological storage (typically represented  
100 as water table). In cases where there is a need for more focus on soil matrix hydrology and less  
101 need for understanding hydrological processes at the catchment scale and the relative  
102 contribution of tiles (and its interplay), modellers tend to use specialised porous-media PDE-  
103 based (partial differential equation-based) numerical models such as HYDRUS (Simunek et al.,  
104 2011) and MACRO (Larsbo and Jarvis, 2003).

105 The amount of water transported by tiles depends on soil moisture dynamics and the  
106 positioning of the water table, which are in turn affected by many factors, including soil type,  
107 surface topography and morphology, as well as the local climate and the hydrological  
108 characteristics of the field (Frey et al. 2016; Klaiber et al., 2020; Coelho et al., 2012; King et al.,  
109 2015). Thus, to provide reliable estimations of water loss from farmland via surface runoff and  
110 tile flow, models must be able to predict soil moisture storage and the water table position  
111 elevation accurately (Brockley, 1976; Rozemeijer et al., 2016; Javani-Jouni et al., 2018). Many  
112 studies have shown that in some soil types, including silty loam and clay loam soils, the  
113 drainable water is less than expected based on the effective porosity (*e.g.*, Skeggs et al., 1978;

114 Raats and Gardner, 1974). Raats and Gardner (1974) have argued that the calculation of  
115 drainable porosity requires knowledge of water table ~~position-elevation~~ and the distribution of  
116 soil moisture above the water table. Skaggs et al. (1978) added that the calculation of drainable  
117 porosity should ~~take-into-account~~consider “the unsaturated zone drained to equilibrium with the  
118 water table”. However, because the soil column is often composed of different soil layers with  
119 varying physical characteristics, drainable porosity varies with evapotranspiration rate, soil water  
120 dynamics and the depth of saturated water (Logsdon et al., 2010; Moriasi et al., 2013). In a sandy  
121 loam soil, Lam et al. (2016a, 2016b) demonstrated that tile drainage was not initiated until soil  
122 was at or above field capacity. Williams et al. (2019) observed in the American Midwest that tile  
123 drainage was not initiated until the field storage capacity had been exceeded. It has also been  
124 shown that despite the presence of tile drains, the soil above the tile may not always drain all  
125 gravitational water following a rainfall/snowmelt event and the soil may remain at or above field  
126 capacity (Skaggs et al., 1978; Lam et al., 2016a). Therefore, the soil drainable water content may  
127 be considerably smaller than the storage capacity. This is related to matric potential within the  
128 vadose zone, which is driven by the soil characteristics but can also be due to the development of  
129 a capillary fringe that reduces the rate of vertical percolation through the unsaturated zone,  
130 reducing tile flow (Youngs, 2012). Despite this evidence, some saturated flow models that  
131 simulate tile flow overlook the effect of capillary rise and over-estimate the soil drainable water.  
132 Other models that represent unsaturated flow (i.e., HYDRUS 3D, Simunek et al., 2011) using  
133 Richard’s Equation (Richards, 1931) capture the effect of capillary rise and saturation-pressure  
134 variation within the soil profile and assess the soil drainable water more accurately. Although the  
135 effect of capillary rise is considered in DRAINMOD through the concept of drainable porosity  
136 (represented as a “water yield”) (Skaggs, 1980b), and is calculated for layered soil profiles

137 (Badr,1978), it requires detailed information surrounding the soil water characteristic curve  
138 (Skaggs, 1980b). Although it is indeed optimal to use soil-specific water characteristic curves,  
139 Twarakawi et al. (2009) found that it was possible to employ average representative values from  
140 the soil water characteristic curve to represent soil drainable water where a soil-specific curve  
141 was not available. They found in this case that the model performance was reduced.

142 In this study, a new ~~tile-Tile drainage-Drainage module-Module~~ **(TDM)** was developed  
143 and incorporated within the physically based, modular Cold Regions Hydrological Modelling  
144 (CRHM) platform (Pomeroy et al., 2022) to enable hydrological simulations in tile-drained farm  
145 fields in cold agricultural regions. As a first iteration, the new module was developed for a field  
146 with sloping ground and loam soil with imperfect drainage. Such landscapes are common in the  
147 Great Lakes Region (e.g., Michigan and Vermont, USA and Ontario, Canada) and tile drainage  
148 in such landscapes has not been as widely studied as it has been in clay-dominated soil. In this  
149 module, considerations were explicitly included for the effects of capillary rise and annual  
150 groundwater water table fluctuations on drainable soil water storage. The use of field capacity  
151 and groundwater/soil water elevation head (Twarakawi et al., 2009) to modulate soil drainable  
152 water across the soil profile, including the capillary fringe region, is an innovative aspect of the  
153 model that has been demonstrated to circumvent the need for water characteristic curves. The  
154 development of this physically based module provides insight into hydrological processes in tile  
155 drainage from sloping landscapes with imperfect drainage, which are increasingly being  
156 artificially drained.

157

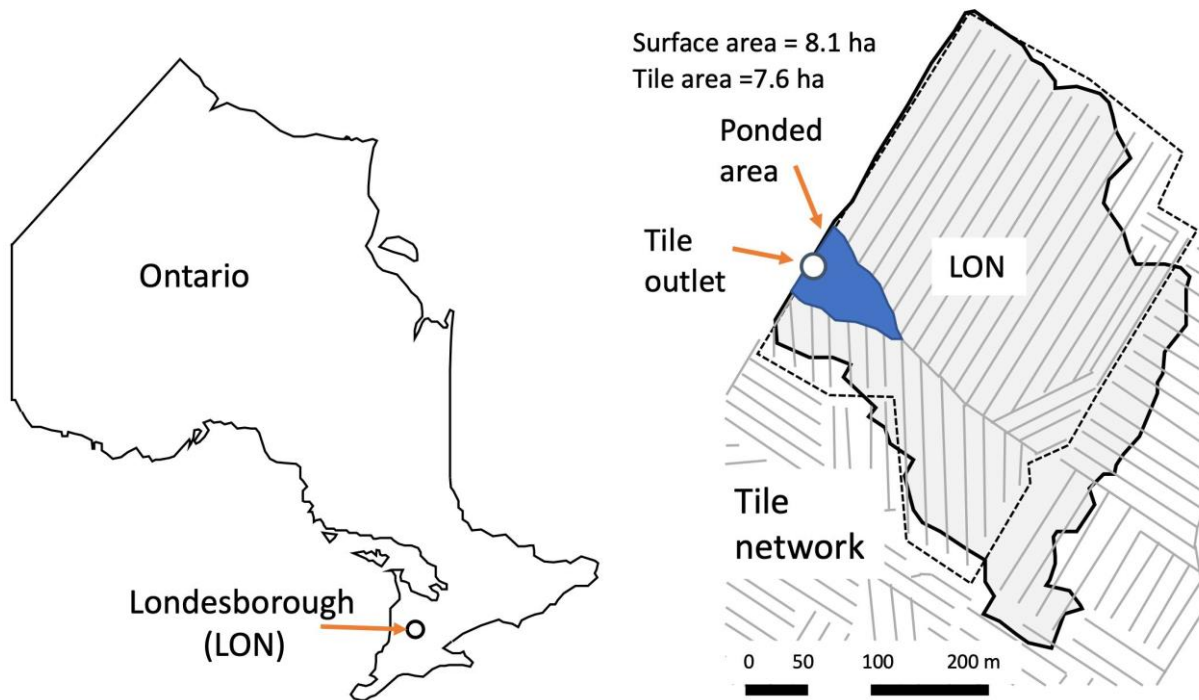
## 158 2. Materials and Methods

### 159 2.1 Study area

160 The study site is a ~10 ha farm field located near Londesborough, Ontario at UTM 17T 466689m  
161 E, 4832203m N, shown as LON in Fig. 1a. Mean annual precipitation recorded in this region is  
162 1247 mm (ECCC, 2020). Mean air temperature is 7.2 °C, with annual maxima in July (25.9 °C)  
163 and minima in January (-10.2 °C), (ECCC, 2020). Soil texture has been identified as Perth clay  
164 loam (Gr. Br. Luvisolic), with a slope between 0.2 and 3.5%. The field is systematically drained  
165 with a tile depth of 0.9 m and a spacing of 14 m (laterals). The tile network collects infiltrated  
166 water from about 75% of the field (~ 7.6 ha) but may also receive lateral groundwater flow from  
167 neighbouring fields. Water yields from the tile drain laterals (10 cm diameter) are discharged via  
168 a common tile outlet (main, 15 cm diameter) below ground. Surface runoff from the field is  
169 directed toward a common outlet on the surface using plywood berms installed along the field  
170 edge (see van Esbroeck et al., 2016). The tile and surface runoff outlets do not join into a  
171 common outlet and are fully separated from one another, even during surface ponding events.  
172 The field is a corn-soy-winter wheat rotation with cover drops and rotational conservation till  
173 (shallow vertical tillage every three years). Additional details related to farming practices are  
174 provided in Plach et al. (2019), soil characteristics are provided in Plach et al. (2018a) and Plach  
175 et al. (2018b) and equipment and monitoring are provided in van Esbroeck et al., (2016). The  
176 outlets for both surface and tile flow are located at the edge of the field and drain into an adjacent  
177 field (Fig. 1b). Water tends to accumulate in a topographic low in the field, in front of the field  
178 outlet during snowmelt or high-intensity rainfall events, presumably due to either surface runoff  
179 or return flow (see ponded area, Fig. 1b). However, surface water or elevated soil moisture  
180 conditions are not observed in this topographic low during smaller events or dry periods of the



181 year, suggesting that this saturated ponding is not in a perennial groundwater discharge zone.  
182 Although surface ponding is observed in the topographic depression within the field, water  
183 discharges freely at the opposite end of the culvert, facilitating the measurement of flow.  
184



185  
186 a)  
187 b) Figure 1. (a) Location of the study area in South of Ontario and the (b) Londesborough (LON) farm with its tile network.  
188  
189

## 190 2.2 CRHM: The modelling platform

191 The modular CRHM platform includes options for empirical and physically based calculations of  
192 precipitation phase, snow redistribution by wind, snow interception, sublimation, sub-canopy  
193 radiation, snowmelt, infiltration into frozen and unfrozen soils, hillslope water movement, actual  
194 evapotranspiration, wetland fill and spill, soil water movement, groundwater flow and

195 streamflow (Pomeroy et al., 2007; 2022). Where appropriate, it calculates runoff from rainfall  
196 and snowmelt as generated by infiltration excess and/or saturated overland flow, flow over  
197 partially frozen soils, detention flow, shallow subsurface flow, preferential flow through  
198 macropores and groundwater flow. Water quality can also be simulated [in CRHM](#) (Costa et al.,  
199 2021). Modules of a CRHM model can be customized to basin setup, such as delineating and  
200 discretizing the basin, conditioning observations for extrapolation and interpolation in the basin,  
201 or are process-support algorithms such as for estimating longwave radiation, complex terrain  
202 wind flow, or albedo dynamics, but most modules commonly address hydrological processes  
203 such as evapotranspiration, infiltration, snowmelt, and streamflow discharge. CRHM discretizes  
204 basins into hydrological response units (HRU) for mass and energy balance calculations, each  
205 with unique process representations, parameters, and position along flow pathways in the basin.  
206 HRU are connected by blowing snow, surface, subsurface and groundwater flow and together  
207 generate streamflow which is routed to the basin outlet. The size of TDM HRUs is flexible and  
208 can be as small as the size of a single tile pipe (e.g., 1 m) times the pipe spacing (which was 14  
209 m in our case study region), and as large as entire tile networks within a given farm or study  
210 area. CRHM does not require a stream within a modelled basin. The feature allows CRHM to  
211 model the hydrology of cold regions dominated by storage and episodic runoff, such as  
212 agricultural fields.

213         Although CRHM has the capability to represent many hydrological and thermodynamic  
214 processes, not all processes need/must be represented in all situations. The modular design of the  
215 CRHM platform enables the user to activate or inactive specific processes to optimize the model  
216 for a particular situation. This is a modelling approach that enables testing different modelling  
217 hypotheses and has been pioneered by CRHM and other models, which has inspired a range of

218 hydrological (e.g., SUMMA, Clark et al., 2015a, 2015b), hydrodynamic (e.g., mizuRoute,  
219 Mizukami et al., 2015) and biogeochemical (e.g., OpenWQ, Costa et al., 2023a, 2023b)  
220 modelling tools. For example, in the current study, blowing snow was not employed in CRHM as  
221 it does not appear to be significant at the study site (periodic snow surveys showed relatively  
222 uniform snow cover). Preferential flow into tile drains was not developed for the current  
223 simulation as although it is a key process in ~~heavy-clay~~ loam soil, as it does not appear to be a  
224 significant driver of preferential flow into tile drains in coarse textured soil (Pluer et al., 2020;  
225 Macrae et al., 2019). Freeze-thaw processes in soil were also not employed here as there is very  
226 little seasonal soil frost in the temperate Great Lakes region due to the persistent snow cover, and  
227 where soil frost occurs, it is restricted to brief periods and shallow depths (above 10 cm depth)  
228 (Macrae unpublished data).

229

### 230 2.3 *Observations and input data for the model*

231 Tile flow, water table ~~position-elevation~~ (water table elevation head) and surface flow were  
232 measured at the site between Oct. 2011 and Sept. 2018 at 15-minute intervals. It was not possible  
233 to install more than one measuring station for water table ~~position-elevation~~ and soil moisture at  
234 the site due to farming activity; consequently, water table elevation head and soil moisture were  
235 measured at the approximate midpoint of the field at the edge-of-field. Both tile flow rates and  
236 surface runoff were determined using simultaneous measurements of flow velocity and water  
237 depths in each of the pipes at the edge-of-field using Hach Flo-tote sensors and an FL900 data  
238 logger (Onset Ltd.) (Table A1, Appendix A). Continuous measurements of velocity were  
239 included due to the potential for impeded drainage under very wet conditions or caused by the  
240 accumulation of snow and ice around the surface culvert in winter. An additional barometrically-

241 corrected pressure transducer (U20, Onset Ltd.) (Table A1) was also used for periods when the  
242 flow sensors did not function using a rating curve developed from the depth-velocity sensors.  
243 The water table ~~position~~ elevation was measured using a barometric pressure-corrected pressure  
244 transducer (U20, Onset Ltd.).

245 Air temperature, wind speed, air relative humidity, incoming solar irradiance and rainfall  
246 were also measured at the site at 15-minute intervals and used to force the model. Variable  
247 names and their symbols in CRHM are listed in Appendix B. The air temperature, wind speed  
248 and incoming solar radiance measurements were collected 1 m above ground using a  
249 Temperature Smart Sensor S-THB-M002, Wind Smart Sensor Set S-WSET-M002 and a Solar  
250 Radiation Sensor (Table A1). Rainfall and relative humidity were measured via a tipping bucket  
251 rain gauge (Table A1) and an RH Smart Sensor (Table A1). These observations were  
252 continuously recorded throughout the study period, except for brief periods of instrument failure  
253 and maintenance, when data from nearby stations (Table T1, Supplementary Material) was  
254 substituted using the double mass analysis method (Searcy and Hardison, 1960).

255 Although rainfall was recorded continuously at the field site, snowfall data was not.  
256 Snowfall data was obtained from nearby stations (Wroxeter-Davis and Wroxeter, Environment  
257 Canada, 2021), located 31.7 km from the field site. Periodic snow surveys done at the site  
258 throughout the study period found that data from the nearby stations was a close approximation  
259 of snow at the field site (Plach et al., 2019). Hourly snowfall observations from Wroxeter-  
260 Geonor were used for the period between 2015 and 2018, whereas daily data from the Wroxeter-  
261 Geonor were used for the 2011 to 2014 period, reconstructed to hourly snowfall time series  
262 based on the method presented by Waichler and Wigmosta (2003).

263

264 2.4 Development of the new tile module

265 A Tile Drainage Module (TDM) was developed within CRHM ([Figures 2, 3](#)) with the goal of  
266 adding the ability to simulate tile flow and the resulting saturated storages (water table) at an  
267 hourly time [scalestep](#). CRHM was forced with hourly precipitation, air temperature, solar  
268 radiation, wind speed and relative humidity to calculate hydrological states and fluxes in HRUs  
269 and the basin. The model requires parameterizations that specify the hydraulic and hydrological  
270 properties of the soil, including its thickness, saturated hydraulic conductivity (K), and surface  
271 cover. CRHM calculates water storage and fluxes between HRUs, as well as vertical fluxes  
272 amongst different hydrological compartments (within each HRU) that include snow,  
273 depressional storage, different soil layers, and groundwater.

274 Using the simulation of soil moisture ([including both saturated and unsaturated soil](#)  
275 [moisture](#)) performed by the original CRHM “Soil” module, TDM calculates the dynamic tile  
276 flow rate that, in turn, feeds back to soil moisture at each time step. The presence of a capillary  
277 fringe (sometimes referred to as the tension-saturated zone within the soil profile) and its effects  
278 are considered by limiting the amount of drainable soil water. TDM uses site-specific  
279 information regarding the tile network, such as tile depth, diameter and spacing. Information  
280 regarding site-specific details regarding tile depth, diameter and spacing may be obtained  
281 directly from landowners or can be estimated based on standard design and installation  
282 guidelines for the region. This information was used to set up the model together with  
283 parameterization to translate the hydrological effects of the soil capillary fringe (CF), if present,  
284 through two [state](#)-variables, CF thickness and CF drainable water (discussed in Section 2.5,  
285 [Figures 2, 3](#)). These two [state](#)-variables are used to limit the fraction of the soil moisture that can  
286 freely drain to the tiles.

287

288 2.4.1 *Soil moisture and water table ~~position~~elevation*

289 The TDM uses the water quality soil module or soil module (*WQ\_soil* or *Soil*), which divides the  
290 soil column into two layers: a recharge layer where evapotranspiration and root uptake generally  
291 take place and a deeper layer that connects to the groundwater system. Since CRHM's state  
292 variable for soil moisture is soil water storage volume (Fig. 2a), the model results were converted  
293 into water ~~level~~table elevation above the semi-permeable layer (Table B1, Appendix B; see Fig.  
294 2b for comparison with water table observations) by dividing volumetric soil moisture content  
295 (Table B1) by soil porosity (Table B1) for the cases with no capillary fringe above the water  
296 table. Additional steps were taken for periods when a capillary fringe developed (discussed  
297 below).

298

299 2.4.2 *Capillary fringe and drainable water*

300 Soil moisture in the capillary fringe is equal to the average volumetric water content at field  
301 capacitycapillary fringe  $-(\theta_{cfe})$  which is usually greater than the ~~more than~~ field capacity ( $\theta_{fc}$ )  
302 (Bleam, 2017, Sect. 2.4). Therefore, while the positioning of the capillary fringe responds  
303 dynamically to the matric potential, the saturation profile within the capillary fringe remains  
304 constant, as well as its thickness because it only depends on the pressure head (capillary forces)  
305 that are related to the grain size distribution and field capacity ( $h_{fc}$ ) as introduced by Twarakawi  
306 et al. (2009). Therefore, the drainable water in the capillary fringe becomes the difference  
307 between saturation ( $\theta_s$ ), computed dynamically in CRHM, and  $\theta_{fec}$ , which corresponds to the  
308 water held by capillary forces at the field capacity capillary fringe moisture content (Fig. 2).

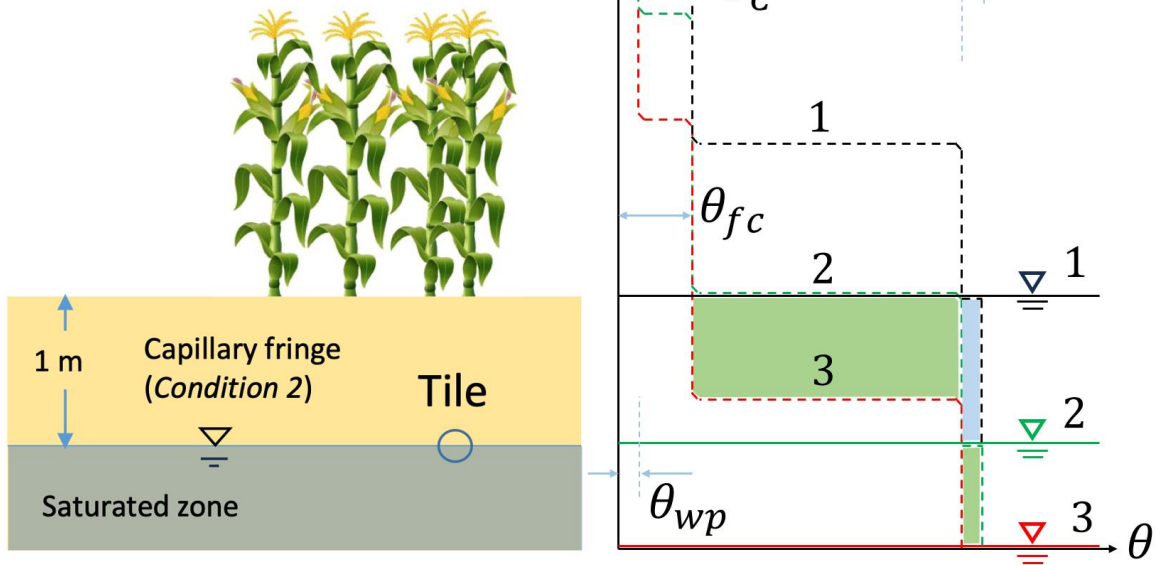
309 Accordingly, Fig. 2 shows the schematic soil characteristic curve for the three water level  
310 conditions contemplated in the model.

- 311 1. *Condition 1* is when the ~~matric head~~water table is at the surface and the soil is  
312 completely saturated (matric potential = 0);
- 313 2. *Condition 2* is when the ~~matric head~~water table drops but the upper boundary of the  
314 capillary fringe is at the soil surface; and
- 315 3. *Condition 3* is when the water table drops ~~further~~further, and the upper boundary of the  
316 capillary fringe drops beneath the surface.

317 In essence, the soil is completely saturated ( $\theta_s$ ) in *Condition 1*. Between *Conditions 1* and 2, the  
318 capillary fringe occupies the entire soil column above the water level; thus, it can only release  
319 the volume of water corresponding to  $\theta_s - \theta_{f\epsilon C}$  or  $\varphi_c$  (dimensionless). Between *Conditions 2* and  
320 3, two layers with distinct hydraulic characteristics develop: (1) the top one at  $\theta_{wpfc}$  that releases  
321 water up to  $\theta_{f\epsilon C} - \theta_{wpfc}$ , and (2) the lower one that corresponds to the capillary fringe and can  
322 release up to the volume of water corresponding to  $\theta_s - \theta_{f\epsilon C}$  or  $\varphi_c$ .

Drained water when the water table position is changed:

- from *Condition 1* to *Condition 2*
- from *Condition 2* to *Condition 3*



323

324 Figure 2. Schematic representation of the capillary fringe above the water table assuming a 1-m thickness (for demonstration  
 325 purposes). The soil characteristic curves are shown for the three water level conditions considered: water level at the (1) surface,  
 326 (2) intermediate depth, and (3) deeper depth. Two transitional drops can be seen in the characteristic curves, one from saturation  
 327 ( $\theta_s$ ) to field capacity-capillary fringe water content ( $\theta_{fc}$ ) (between *Conditions 1* and 2) and one from field capacity- $\theta_c$  to field  
 328 capacity-wilting point ( $\theta_{wp}$ ) (between *Conditions 2* and 3). The coloured areas (green and blue) of the right panel correspond to  
 329 the amount of water that can be released between *Conditions 1* and 2 (blue) and between *Conditions 2* and 3 (green).

330

331

### 332 2.4.3 Tile flow calculation

333 A modified version of the Hooghoudt equation was used to calculate tile flow (Smedema et al.,  
 334 2004), which presumes no surface ponding, an assumption that generally holds at the study site  
 335 (Eq. 1), where water ponds only during very wet periods and on a small portion of the study site  
 336 (see Fig. 1b). Hooghoudt's equation (Hooghoudt, 1940) is a steady state, physically based



337 equation for saturated flow toward the tile drain. Flow estimates are provided based on the  
 338 hydraulic conductivity of the soil and ~~matric potential~~water table elevation above the tile pipe. It  
 339 allows different saturated hydraulic conductivities for the layers above (AL) and below (BL) the  
 340 tile (Fig. S1). ~~In~~At the ~~particular case of the case~~ study site, soil surveys have reported almost  
 341 the same soil type (Loam) down to the depth of 90 cm (*e.g.*, Van Esbroeck et al., 2016; Plach et  
 342 al., 2018b), which was parameterized in the model set up as,

343

$$344 \quad q = \frac{8 \times K_2 \times d \times h}{L^2} + \frac{4 \times K_1 \times h^2}{L^2}, \quad (1)$$

345

346 where  $K_1$  and  $K_2$  are respectively the saturated hydraulic conductivity in the upper and lower  
 347 layers in  $\text{mm h}^{-1}$ ;  $L$  is the tile spacing in mm;  $h$  is the water table elevation above the tile in mm,  
 348  $d$  is the lower layer thickness in mm (Fig. S1), and  $q$  is the predicted tile flow in  $\text{mm h}^{-1}$ . The  
 349 only variable that is dynamically updated by CRHM is  $h$ . Equation (1) is used to estimate the tile  
 350 flow.

351

#### 352 2.4.4 Calculation of the effect of tile flow on soil moisture and water levels

353 The simulated tile flows (see Sect. 2.3.3) are subtracted from the soil moisture. To calculate  
 354 saturated storage (water table or groundwater elevation head level) from soil moisture calculated  
 355 by the model, a threshold soil moisture content ( $sm_t$ ) is defined, which consists of drainable  
 356 water in the soil ( $\varphi_c$ ) when the upper boundary of the capillary fringe is at the surface (*Condition*  
 357 2, Fig. 2) and was calculated as:

358

$$359 \quad sm_t = sm_{max} - (C_t \times \varphi_c), \quad (2)$$

360

361 where  $sm_{max}$  is the maximum soil moisture and  $C_t$  is the capillary fringe thickness in mm.

362 However, since the hydrological conditions of the soil are markedly different between the two

363 transitional situations described in Sect. 2.3.2 and Fig. 2 (*Condition 1* to 2 and *Condition 2* to 3),

364 a step function was deployed- for determination of the matric potential water table elevation:

365

366

$$WT = \begin{cases} \frac{sm_t - (C_t \times ((\varphi_s - \varphi_c) + \theta_{wpfc}))}{\varphi_s + \theta_{wpfc}} + \frac{sm - sm_t}{\varphi_c} & , \text{if between Conditions 1 and 2} \\ \frac{sm_{max}}{\varphi_s + \theta_{wpfc}} - \left( \left( \frac{sm_t - sm}{\varphi_s} \right) + C_t \right) & , \text{if between Conditions 2 and 3} \end{cases} \quad (3)$$

367

368 where  $WT$  is water table elevation (or soil saturated storage, SSS) in mm from the bottom of the

369 soil, and  $sm$  is soil moisture (both saturated and unsaturated storage) in the given time step in

370 mm. Equation (3) is determined based on soil moisture curves in Fig. 2 and water level

371 *Conditions 1-3* discussed in Sect. 2.3.2. In Fig. 2, the first and second parts of Eq. (3), which

372 refer to *Conditions 1* to 2 and 2 to 3, respectively, correspond to the volumes of soil water

373 highlighted in “blue” and “green.”

374

#### 375 2.4.5 Lower semi-permeable soil layer and periodicity in annual groundwater levels

376 This model application focused on the study site field without including other adjacent areas.

377 This was possible because years of field monitoring at this site have demonstrated that there is no

378 observable surface flow into the site from adjacent farms. The tile network is restricted to the

379 field and is not connected to tile drains or surface inlets in adjacent fields. However, field soil

380 water table observations show evidence of annual groundwater level periodicity/fluctuation (Rust

381 et al., 2019) that are sinusoidal in nature and cannot be neglected. Some studies predict the  
 382 annual groundwater oscillations or the annual responses of groundwater to precipitation by using  
 383 sine and cosine functions (De Ridder et al., 1974; Malzone et al., 2016; Qi et al., 2018). De  
 384 Ridder et al. (1974) studied the design of the drainage systems and described the seasonal  
 385 groundwater fluctuations observed in wells using sinusoidal curves. Malzone et al. (2016) used a  
 386 sine function to predict annual groundwater fluctuations in the hyporheic zone. Qi et al. (2018)  
 387 and Rust et al (2019) used a cross-wavelet transform, consisting of the superposition of sine and  
 388 cosine curves, to predict shallow groundwater response to precipitation at the basin scale. This  
 389 approach was used in this application to simulate annual fluctuations in groundwater water  
 390 tables, in Eq. (4), ~~with over~~ a period of 1 year, ~~with~~ minimums around the middle of the growing  
 391 season (mid-July), and maximums in the cold season (early February). This translates into the  
 392 ~~lowering of the~~ matric potential during the growing season, ~~coinciding with soil moisture~~  
 393 ~~depletion lower soil moisture causing soil water seepage~~, and ~~then an elevated matric potential~~  
 394 during the non-growing season, ~~an elevated matric potential causing coinciding with~~ an increase  
 395 in the soil moisture, consistent with field observations. Thus, a sine function representing the  
 396 annual fluctuations in ~~percolation rate from soil to groundwater water table~~ ( $G_{y,i}$ ) ~~layers in~~  
 397 ~~CRHM, through the lower soil semi-permeable layer (in mm hr<sup>-1</sup>) which~~ is defined as ~~below~~:

398

$$399 \quad G_{y,i} = \left[ A \times \sin \left( \frac{(T_s - D_d \times 24) \times 360}{24 \times 365.25} \right) - B \right] \times f_{y,i} \quad (4)$$

400

401 where  $T_s$  is the time step number,  $D_d$  is a time delay in days,  $A$  is the amplitude of the ~~soil~~-water  
 402 table (WT ~~or~~ /SSS) fluctuation, and  $B$  is an intercept factor.  $f_{y,i}$  is a seasonal factor. The sine  
 403 function coefficient ( $D_d$ ,  $A$ , and  $B$ ) and seasonal factor were adjusted for the whole period and

404 for each year through model verification and shown in Table 1. Appendix C provides more  
405 details on the implementation of Eq. (4).

406

### 407 2.5 *Model application and multi-variable, multi-metric validation*

408 The study site is a relatively small field, and 2 HRUs were sufficient to capture its hydrological  
409 dynamics in CRHM. The HRUs represent (1) the area immediately upstream of the outlet where  
410 surface ponding occurs (depression storage); and (2) the remaining field (Fig. 3). The maximum  
411 ponding capacity of HRU 1 was estimated using the spatially distributed hydrodynamic model  
412 FLUXOS-OVERFLOW (Costa et al., 2016, 2020b). The CRHM model ~~with its~~ new TDM  
413 module were set up using the information described in Table 1. Soil textures at the LON site  
414 measured in a 25 m grid across three soil depths (0-25 cm, 25-50 cm, and 50-100 cm) averaged  
415 29% sand, 48% silt, and 23% clay (Ontario Ministry of Agriculture, Food and Rural Affairs Soil  
416 Team, unpublished data). This soil grain size distribution corresponds with a soil-saturated  
417 hydraulic conductivity of  $\sim 0.56 \text{ cm h}^{-1}$  ( $\sim 10^{-2.5}$ ) (Garcia-Gutierrez et al., 2018), which was  
418 implemented in CRHM ( $0.5 \text{ cm h}^{-1}$ ), corresponding to a field capacity of ~~0.03-04~~ (volumetric  
419 water content) and  $h_{fc}$  of  $\sim 0.8 \text{ m}$  (Twarskawi et al., 2009, based on a drainage flux of  $0.1 \text{ cm d}^{-1}$ ).  
420 <sup>1</sup>).

421

422 A robust multi-variable, multi-metric model evaluation strategy was deployed to verify the  
423 capacity of the model to predict tile flow and its impact on the local hydrology. The ~~state~~  
424 variable outflows examined were tile flow, surface flow, and ~~matric potential~~ water table depth.  
425 The multi-metric approach contemplated five different methods, namely the Nash-Sutcliffe  
426 efficiency (*NSE*), Root-Mean-Square Error (RMSE), Model Bias (Bias), Percentage Bias

427 (PBias), and RMSE-observation standard deviation ratio (RSR). See Appendix C for more details  
428 about the methodology used. It is generally assumed that  $NSE > 0.50$ ,  $RSR \leq 0.70$ , and  $PBias$  in  
429 the range of  $\pm 25\%$  are satisfactory for hydrological applications (Moriassi et al., 2007). We used  
430 five different metrics were used to evaluate model accuracy in order to describe as they show  
431 different aspects of the discrepancies between simulated and observed values. For example, Bias  
432 reveals the positive or negative general deviations of simulated values from the observed values,  
433 while RMSE shows the average absolute differences between them (Moriassi et al., 2007). Hourly  
434 values were used in these calculations, which departs from the daily and monthly analyses  
435 typically reported for these types of models. Although the hourly timestep ~~this is a~~ challenging  
436 for this sort of simulation ~~proposition~~, it is an important advance ~~one as it constitutes a necessary~~  
437 step forward toward more detailed, accurate, and advanced models for tile drained agricultural  
438 fields ~~these regions~~. For example, Costa et al., (2021) noted that the successful extension of  
439 hydrological models to water quality studies relies on their ability to operate at small time scales  
440 in order to capture intense, short-duration storms that may have a disproportional impact on the  
441 runoff transport of some chemical species such as phosphorus – in essence, to capture hot spots  
442 and hot moments for flux generation.

443

444

445 Table 1. Key model parameters in CRHM for representation of the LON site.

446

Model Parameter	Value	Unit	Source	Adjusted/Calibrated	Comment
Soil depth <u>or Soil thickness, <math>T_{SL}</math></u>	2	m		No	Assumed
Semipermeable layer depth	3	m		No	Assumed

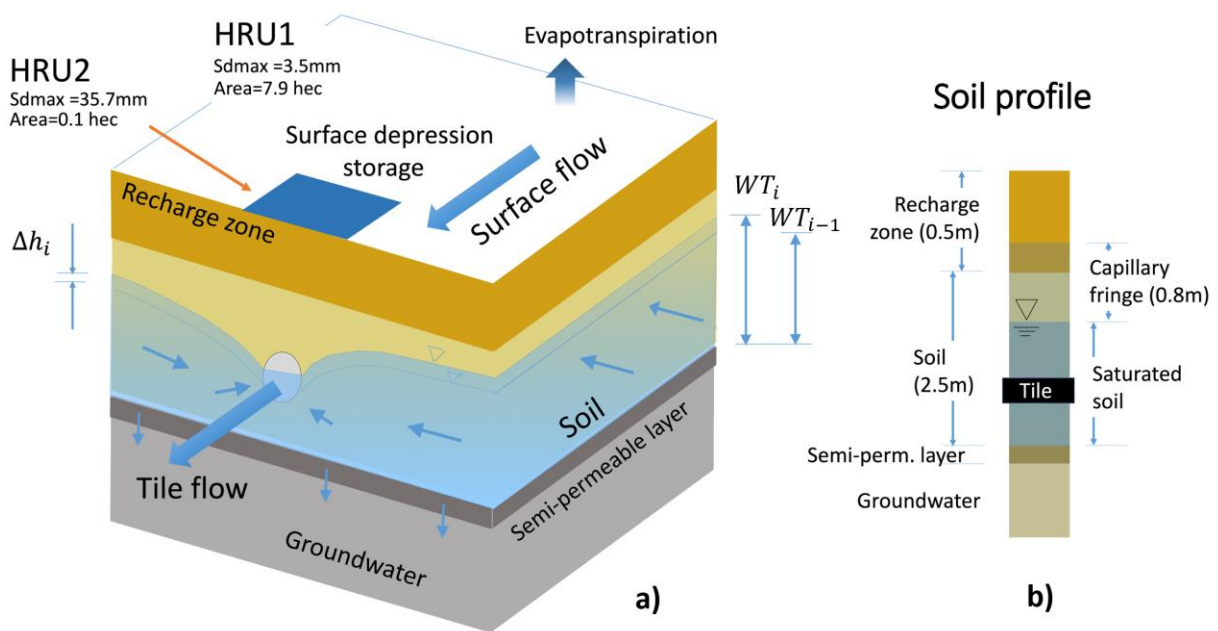
Tile depth	0.9	m	No	Farmer/Blueprints of the field
Corn root depth	0.5	m	No	Online sources
Soil recharge zone thickness	0.5	m	No	Based on the root depth
Tile spacing	14	m	No	Farmer/Blueprints of the field
Soil porosity (soil drainable water)	0.045		Yes	Adjusted
$\varphi_s$				
<u>Saturated Hydraulic conductivity</u> , $K$ in <u>lower soil</u> layer	5	mm h <sup>-1</sup>	Yes	Adjusted
$K$ in <u>upper soil</u> layer	5	mm h <sup>-1</sup>	Yes	Adjusted
Capillary fringe thickness, $T_{CF}$	0.8	m	Yes	Adjusted
Capillary fringe drainable water, $\varphi_c$	0.03		Yes	Adjusted
Surface depression <u>in small area</u> close to farm surface flow outlet (HRU2)	35	mm	Yes	Calculated
Surface depression in rest of the <u>field area</u> (HRU1)	0	mm	No	Calculated
Surface area of HRU1	79000	m <sup>2</sup>	No	Field observations and DEM
Surface area of HRU2	1000	m <sup>2</sup>	No	Field observation and DEM
Soil module name in CRHM	WQ_soil		No	
Infiltration module name in CRHM	GreenAmpt		No	
Soil type in GreenAmpt module	5		Yes	Adjusted
Saturated K in GreenAmpt module	6	mm h <sup>-1</sup>	Yes	Adjusted
Soil wilting point	0.025		Yes	Adjusted
A, in sine function	0.025	mm h <sup>-1</sup>	Yes	Adjusted

$B$ , in sine function	-0.005	$\text{mm h}^{-1}$	Yes	Adjusted
$D_d$ , in sine function	15	d	Yes	Adjusted
$f_{2012,2}$ (Seasonal factor, sine function)	2.0		Yes	Adjusted
$f_{2015,2}$ (Seasonal factor, sine function)	1.8		Yes	Adjusted
$f_{2016,2}$ (Seasonal factor, sine function)	2		Yes	Adjusted
$f_{2017,2}$ (Seasonal factor, sine function)	1.4		Yes	Adjusted
$f_{y,i}$	1		No	By default for $y =$ 2012 to 2017 and $i = 1, 2$

447

448

449



450

451 Figure 3. a) Schematic conceptual view of the CRHM model configuration, including soil layers, water table (WT/SSS),

452 groundwater, and tile flow.; and b) soil profile, including the capillary fringe and its location relative to the soil and tile.

453

454 **3. Results**

455

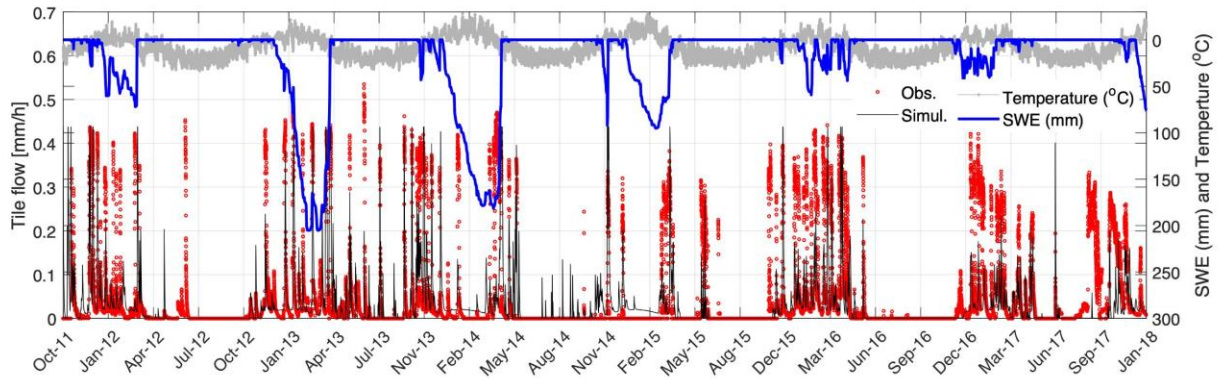
456 *3.1 Tile flow*

457 The model was able to capture most tile flow events, both in terms of the timing and magnitude  
458 of peak flows and the most important seasonal patterns (Fig. 4). For example, the almost  
459 complete absence of tile flow during the growing season (May to September) was captured. The  
460 simulated flow peaks generally had a good agreement with observations, as well as the low flow  
461 or base flows during cold periods (December-March). The ascending and descending limbs of  
462 the response signal were also adequately predicted.

463

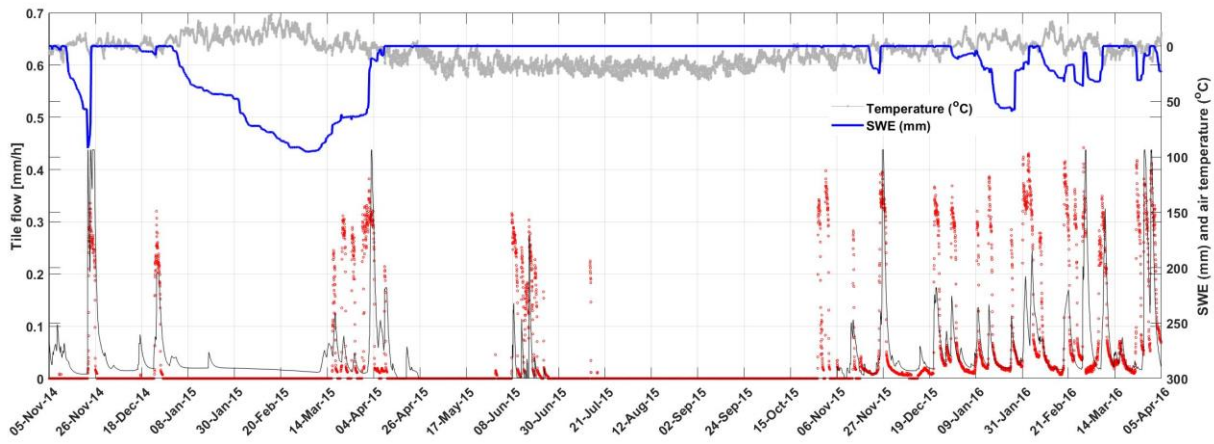
464 Results show that tile flows generally occurred during snowmelt events, as indicated by the  
465 synchrony between snow water equivalent (SWE) depletion and tile flow. The maximum  
466 snowpacks (or snow water equivalent, SWE) were markedly smaller during the winters of 2016  
467 and 2017 when compared with those of 2013 to 2015. However, this did not necessarily translate  
468 into lower tile flows as precipitation also occurred as rain during these seasons. Although the  
469 magnitude of tile peaks was not always ~~assessed-predicted~~ accurately, the model was able to  
470 capture the annual trends of both an absence of tile flow during the summer months (growing  
471 season) and the ascending and descending limbs of the tile hydrograph during events (Figure 4).





472

473 a)



474

475 b)

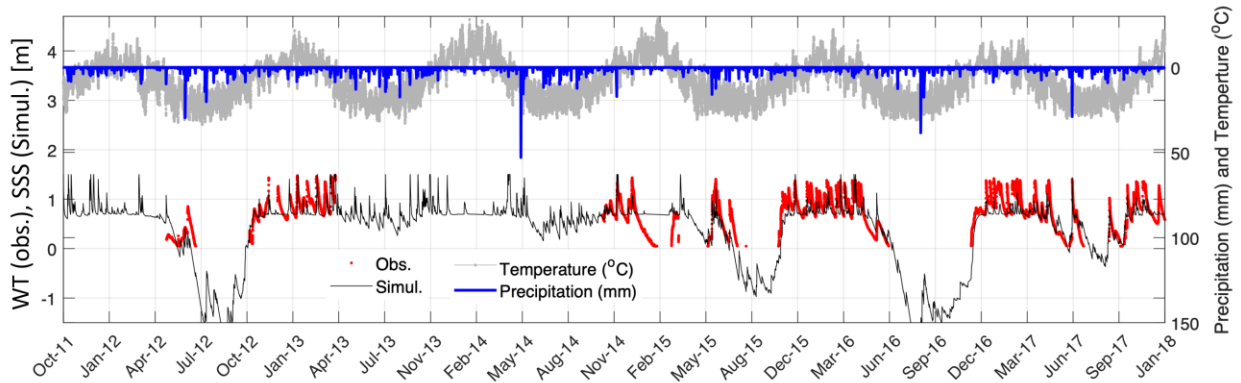
476 Figure 4. Comparison between observed and simulated tile flows, simulated SWE (snow water equivalent), and observed air  
 477 temperature in the LON site, between October 2011 to January 2018 (a) and between November 2014 to April 2016 (b).:-

478

479 *3.2 Water table or soil saturated storage*

480 Simulated soil saturated storage and the observed water table are compared in Fig. 5, alongside  
 481 air temperature and precipitation observations. Despite the gaps in the observational record  
 482 during two periodic equipment failures, gaps, the model agrees well with observations. Above  
 483 tile drains, water table fluctuations were controlled by infiltration/recharge, tile flow,  
 484 groundwater flow, and matric potential that affect the drainable water from the capillary fringe.

485 This causes flashier storage responses above the tile that are captured well by the model. In  
 486 contrast, tiles do not withdraw water from the soil layer below the tile pipe and thus do not  
 487 control water table fluctuations when levels are below the drain pipe, and tile drains simply  
 488 do not flow during such periods. During the growing season, both the observed and simulated  
 489 water table (or saturated storage) drops abruptly because of the seasonal lowering of the  
 490 regional groundwater water table. In the growing seasons of 2012, 2015 and 2016, which were  
 491 dry years, large declines in the water table and saturated storage were observed, whereas in  
 492 wetter years such as 2013 and 2014, seasonal water level declines were smaller. The seasonal  
 493 declines in water level during the growing season led to a cessation in tile flow in most years  
 494 (Fig. 4, 5), even following rainfall events. For example, there was a large precipitation event  
 495 (~35 mm) in the growing season of 2016 that did not produce tile flow (apparent in both model  
 496 and observations).

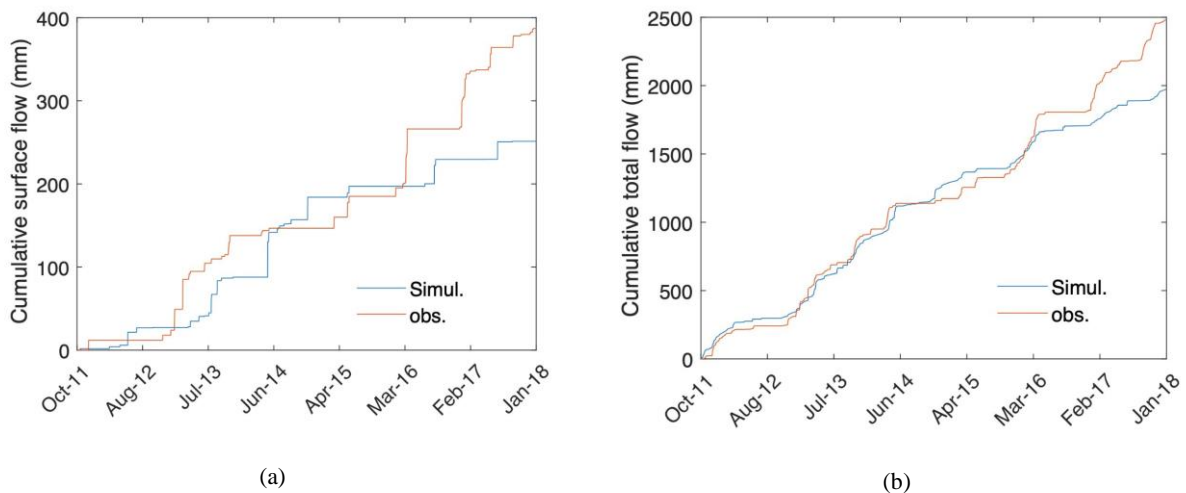


497  
 498 Figure 5. Time series of the simulated saturated storage and observed water table in the soil or groundwater layers of the model  
 499 (soil water table/groundwater table) along with the observed temperature and precipitation. Given that tiles do not flow when the  
 500 WT is below them, the WT = 0 when the water table position/elevation is at the depth of the tile drain-pipe. In the figure, the  
 501 water table is measured as the elevation above (+) or below (-) the tile pipe/horizontal line shows, so tile pipe is located at  
 502 WT=0 the depth of the tile pipe.

503

504 3.3 Surface flow and total flow

505 The model was not always able to capture the observed surface flow as satisfactorily as it  
506 captured tile drainage (Fig. 6a). Some of the possible reasons are uncertainties in the  
507 measurements of surface flow due to ponding in surface depressions on the field, which impeded  
508 the drainage of some of the surface runoff prior to when it exited the field through the culvert  
509 (see Fig. 1), or due to uncertainty in field estimates of SWE. However, the model performance  
510 improves considerably when both runoff and tile flow are combined (referred to as total flow,  
511 Fig. 6b). Indeed, most of the flow from the field was through tile drains (80% in 5-year average)  
512 rather than surface runoff (20% in 5-year average, Plach et al., 2019). The underestimation of  
513 both cumulative total and surface flows during 2017 and 2018 is possibly due to the removal of  
514 the blockage in the tile pipe in early 2017, which may have affected both surface and tile flow.  
515 The differences in timing of the simulated and observed surface flow for many of the main  
516 events (Figure 6) shows that there should be something remain systematic issues in simulation of  
517 surface flow by CRHM, which should be addressed in future research works.



518 Figure 6. Observed and simulated cumulative surface flow (a) and total flow (b) ~~with their performance coefficients.~~

519

520 3.4 Overall model performance

521 The model performance was calculated based on hourly data for various model outputs (Table  
 522 2). The results confirm that the model is robust in the sense that it can capture the main patterns  
 523 of tile flow, surface flow, and ~~matric potential levels~~ water table elevation. The PBias values are  
 524 below 25% for most of the fluxes and cumulative fluxes. The RSR values are also generally  
 525 below 1.0. The NSE values are positive and above 0.3 for most fluxes, except for surface flow,  
 526 where the model exhibited some difficulties. The weaker performance of the model in simulation  
 527 of surface flow which is illustrated shown by the NSE coefficient canshould be partly related to  
 528 difficulties in measurement of surface flow during flooding, ponding and freeze and thaw on the  
 529 surface. We calculated tThe performance coefficients were calculated for May-September (Table  
 530 2b) and October-April (Table 2c). The results shows that surface flow biases are significantly  
 531 larger and negative in May-September and are smaller and positive during October-April. For  
 532 tile flow the Biases are a bit higher in May-September while for soil water table and total flow  
 533 the biases are are a bit lower in May-September. The NSEs are more acceptable in October to  
 534 April for surface flow, tile flow and total flow but the NSE for WT is more acceptable in May-  
 535 September.

536  
 537 Table 2. Performance coefficients for surface flow, tile flow and water table (WT/SSS), as well as total (tile + surface) flow, for  
 538 the simulation period of October 2011 to January 2018. The coefficients were calculated for both hourly and daily flow rates, for  
 539 the whole year (a) for May to September (b) and for October to April (c). (Green and red color show the seasonal coefficients  
 540 improved and worsened, respectively, compared to their seasonal values).

541 a) Coefficients for whole year

Performance coefficients	Surface flow	Tile flow	WT (SSS) (m)	Total flow

NSE*	-2.29	0.31	0.49	-1.38	Coefficients calculated for hourly flow rates (mm h <sup>-1</sup> )
RMSE <sup>^</sup>	0.27	0.08	0.26	0.30	
Bias <sup>#</sup>	0.54	0.24	0.14	0.28	
PBias <sup>\$</sup>	21.77	17.91	10.46	18.63	
RSR <sup>&amp;</sup>	1.82	0.83	0.71	1.54	
NSE	-0.73	0.29	0.50	0.01	Coefficients calculated for daily flow rates (mm d <sup>-1</sup> )
RMSE	2.04	1.72	0.24	2.92	
Bias	0.35	0.20	0.09	0.22	
PBias	35.11	19.63	9.33	21.73	
RSR	1.31	0.84	0.70	0.99	

542

543

544

## b) coefficients for May to September

<u>Performance coefficients</u>	<u>Surface flow</u>	<u>Tile flow</u>	<u>WT (SSS) (m)</u>	<u>Total flow</u>	
<u>NSE*</u>	<u>-18.98</u>	<u>0.19</u>	<u>0.40</u>	<u>-11.76</u>	Coefficients calculated for hourly flow rates (mm h <sup>-1</sup> )
<u>RMSE<sup>^</sup></u>	<u>0.26</u>	<u>0.03</u>	<u>0.12</u>	<u>0.26</u>	
<u>Bias<sup>#</sup></u>	<u>-1.43</u>	<u>0.49</u>	<u>0.03</u>	<u>0.11</u>	
<u>PBias<sup>\$</sup></u>	<u>-142.79</u>	<u>48.88</u>	<u>3.44</u>	<u>10.96</u>	
<u>RSR<sup>&amp;</sup></u>	<u>2.85</u>	<u>0.57</u>	<u>0.39</u>	<u>2.27</u>	
<u>NSE</u>	<u>-3.89</u>	<u>0.21</u>	<u>0.41</u>	<u>-1.08</u>	Coefficients calculated for daily flow rates (mm d <sup>-1</sup> )
<u>RMSE</u>	<u>1.39</u>	<u>0.73</u>	<u>0.11</u>	<u>1.66</u>	
<u>Bias</u>	<u>-1.43</u>	<u>0.49</u>	<u>0.02</u>	<u>0.11</u>	
<u>PBias</u>	<u>-142.79</u>	<u>48.88</u>	<u>2.07</u>	<u>10.96</u>	
<u>RSR</u>	<u>1.41</u>	<u>0.56</u>	<u>0.39</u>	<u>0.92</u>	

545

546

## c) coefficients for October to April

<u>Performance coefficients</u>	<u>Surface flow</u>	<u>Tile flow</u>	<u>WT (SSS) (m)</u>	<u>Total flow</u>	
<u>NSE*</u>	<u>-0.37</u>	<u>0.24</u>	<u>0.20</u>	<u>-0.04</u>	Coefficients calculated for hourly flow rates (mm h <sup>-1</sup> )
<u>RMSE<sup>^</sup></u>	<u>0.11</u>	<u>0.07</u>	<u>0.21</u>	<u>0.14</u>	
<u>Bias<sup>#</sup></u>	<u>0.87</u>	<u>0.14</u>	<u>0.11</u>	<u>0.24</u>	
<u>PBias<sup>\$</sup></u>	<u>86.59</u>	<u>13.56</u>	<u>11.00</u>	<u>24.11</u>	
<u>RSR<sup>&amp;</sup></u>	<u>0.90</u>	<u>0.67</u>	<u>0.77</u>	<u>0.79</u>	

<u>NSE</u>	<u>-0.11</u>	<u>0.26</u>	<u>0.24</u>	<u>0.18</u>	Coefficients calculated for daily flow rates (mm d <sup>-1</sup> )
<u>RMSE</u>	<u>1.50</u>	<u>1.56</u>	<u>0.21</u>	<u>2.40</u>	
<u>Bias</u>	<u>0.87</u>	<u>0.14</u>	<u>0.11</u>	<u>0.24</u>	
<u>PBias</u>	<u>86.59</u>	<u>13.56</u>	<u>10.58</u>	<u>24.11</u>	
<u>RSR</u>	<u>0.81</u>	<u>0.67</u>	<u>0.75</u>	<u>0.70</u>	

547

548

549

550

551

\*Nash-Sutcliffe efficiency, ^Root-Mean-Square Error, #Model Bias, %Percentage Bias, &RMSE-observation standard deviation ratio

552

### 553 3.5 Presence of capillary fringe: effects and hypotheses

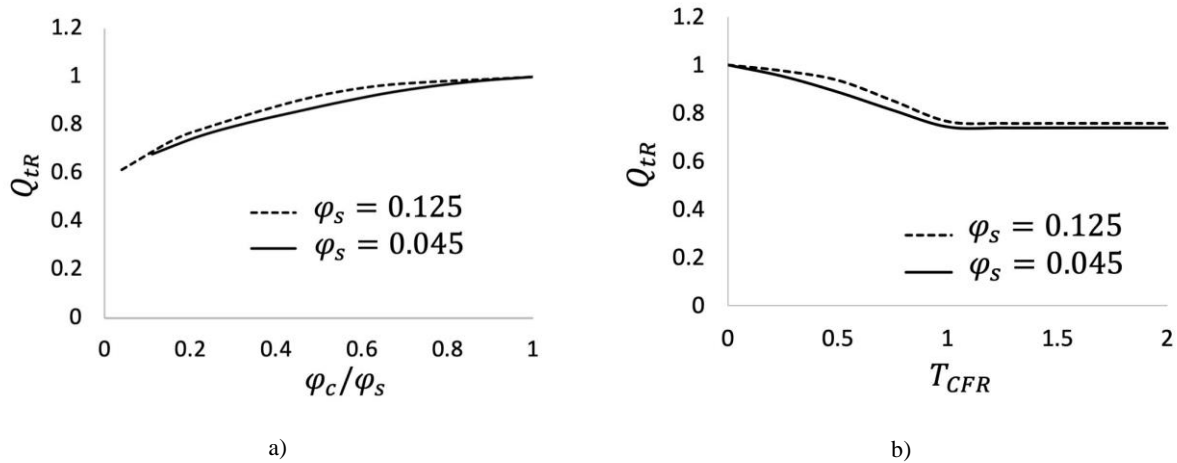
554 Results show that the thickness and vertical positioning of the capillary fringe have a strong  
 555 impact on the amount of drainable soil water that can flow into tiles. To investigate this effect  
 556 further, the response of tile flow and soil moisture to changes in the capillary fringe was  
 557 ~~examined~~investigated. It should be noted that although this thickness may ~~slightly~~change  
 558 ~~slightly~~ depending on the soil type and water retention curves (Skaggs et al., 1978), the model  
 559 assumed a constant value given the ~~catchment~~field-scale nature of the simulations and myriad of  
 560 processes contemplated. However, despite the simplification, the vertical positioning of the  
 561 capillary fringe was still ~~calculated~~computed and enabled a dynamic (time-dependent) calculation  
 562 of the drainable soil water that ~~was~~is available for tile drainage over time.

563

#### 564 Effect of capillary fringe on tile flow

565 Figure 7a relates the simulated normalized total cumulative tile flow ( $Q_{tR}$ , total tile flow divided  
 566 by the total tile flow when there is no influence of capillary fringe) to capillary fringe drainable  
 567 water ( $\varphi_{cR} = \varphi_c/\varphi_s$ ) for two different  $\varphi_s$  values (0.045 and 0.125). The values were

568 normalized (0 - 1 scale) for comparison purposes. As expected, the model indicates that tile flow  
569 increases with drainable water, but the relationship is non-linear, likely because as tile carrying  
570 capacity is exceeded more frequently, there is more opportunity for groundwater seepage and  
571 evapotranspiration. The direct effect of  $\varphi_s$  (comparing the solid and dashed lines) on tile flow is  
572 small because the amount of water that can effectively drain to the tile is controlled by the  
573 capillary fringe and the associated drainable soil water. Figure 7b looks at the impact of the  
574 capillary fringe thickness on tile flow. Here, the values are also normalized. Results show that  
575  $Q_{tR}$  decreases with increasing normalized thickness of the capillary fringe,  $T_{CFR} \left( \frac{T_{CF}}{D_t} \right)$ , capillary  
576 fringe thickness divided by tile depth), but only while the  $T_{CFR}$  is less than 1 that is when the  
577 capillary fringe position is above the tile but has not reached the soil surface. Beyond this point,  
578 increments in the capillary fringe thickness have no impact on tile flow because *Condition 1* has  
579 been reached (see Fig. 2), which essentially means that the capillary fringe has reached the soil  
580 surface. The match between the curves for two different  $\varphi_s$  values shows that the changes in  $\varphi_s$   
581 does not influence the effect of normalized capillary fringe thickness and drainable water on  
582 normalized tile flow. In Appendix D the sensitivity of cumulative tile flow and mean soil water  
583 table elevation to different parameters we are shown along with . Also, in Appendix D the general  
584 approaches for evaluation of the model parameters for new sites, ~~the~~ the site with no tile flow  
585 and water table observations are presented.



586 Figure 7. Comparison between normalized tile flow ( $Q_{tR}$ ) and (a) normalized drainable soil water ( $\phi_c/\phi_s$ ) and capillary fringe  
 587 thickness ( $T_{CFR}$ ) for different maximum soil saturation values ( $\phi_s$ ), by drawing the model prediction lines.  
 588

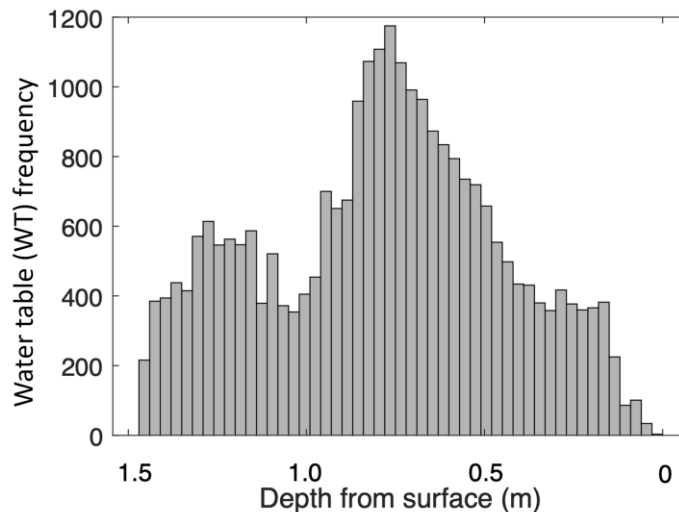
### 589 *Effect of capillary fringe on soil moisture*

590 Observations and model results of WT (~~or SSS as an indicator of soil moisture~~) reveal a bimodal  
 591 frequency distribution (Fig. 8 and 9, respectively) with peaks at 0.85 m and 1.25 m depth, with  
 592 the former corresponding to the depth of the tile pipe and the second peak reflecting capillary  
 593 fringe thickness. In the simulated soil saturated storage (SSS as a measure of WT) frequency  
 594 distributions (Fig. 9), the first peak highlights again the efficiency of the tile in removing soil  
 595 moisture. In contrast, the second peak indicates a strong model response to differences in the  
 596 capillary fringe-fringe thickness. It shows that when there is near-constant discharge-percolation  
 597 from the bottom of the soil layer, the matric potential varies the greatest while it remains  
 598 between the tile depth and the soil surface. While the matric potential water table fluctuates faster  
 599 and is more unstable within this range, it also remains there for shorter periods. This bimodal  
 600 response tends to push the matric potential water table depth below the tile. In Figure 9, we can  
 601 see that the first peak happens at 0.9 m depth where the tile pipe is located, and the second  
 602 peak happens at the depth equal to capillary fringe thickness. In Figure 9 the second peak is ore



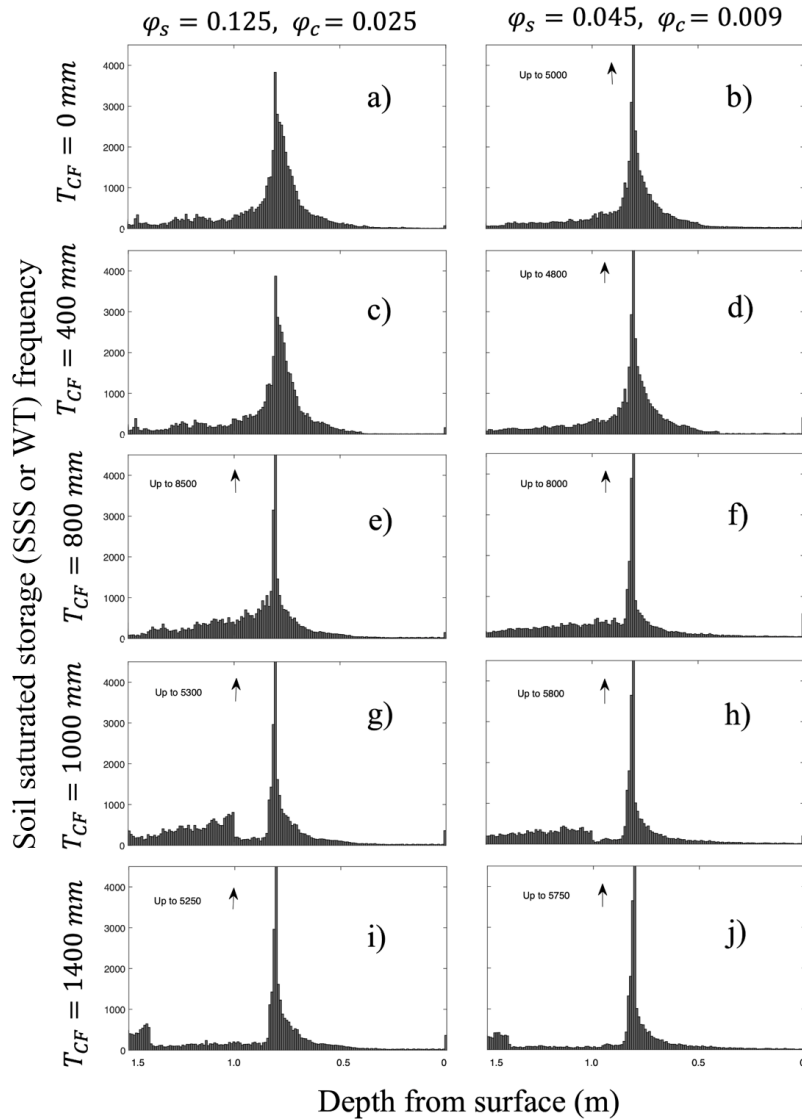
603 clear for the capillary fringe thickness of more than 1000 mm. The first peak in the observed  
604 water table frequency plot (Figure 8) happened around 0.8 m which almost matches with  
605 the tile depth. And the second peak happened at the depth of ~1.2 m which shows that the  
606 capillary fringe thickness should be around 1.2 m. But, to have a more reliable estimated for the  
607 capillary fringe, based on Figure 8, we needed to have data is needed at depths greater than for  
608 more than 1.5 m depth.

610 The bimodal behaviour of the observed water table and simulated saturated storage demonstrated  
611 here provides the opportunity to quantify the thickness of the capillary fringe using continuously  
612 monitored water table position elevations. The capillary fringe thickness determined using this  
613 method can then be used as an input to the TDM module.



614  
615 Figure 8. Histogram of the observed water table distribution for the period of 2011 to 2018 in LON (Londesborough).

616



617

618

619

620

621

#### 622 4. Discussion

623

624

625

Figure 9. Histograms of the simulated soil saturated storages (SSS or WT) for the capillary fringe thicknesses of 0 (a,b), 400 (c,d), 800 (e,f), 1000 (g,h) and 1400 (i, j) mm and for the  $\varphi_s$  and  $\varphi_c$  of 0.125 and 0.025 (left column) as well as 0.045 and 0.009 (right column).

~~The new TDM module developed for CRHM was able to capture tile drainage flow and its effect on the hydrological patterns of a farm field in southern Ontario. This module helps extend the existing capacity of representing the effect of tile drainage in the hydrology of agricultural cold~~

626 ~~regions, from the colder Canadian Prairies to the more temperate Great Lakes region. Tile~~  
627 ~~drainage is prevalent across much of the cultivated lands in the Great Lakes basin and adjacent~~  
628 ~~regions from southern Canada to the upper US Midwest. It is expanding in the eastern Canadian~~  
629 ~~Prairies as well. The new TDM module will also permit simulating the impacts of a changing~~  
630 ~~climate on runoff processes in these landscapes. In addition to this potential, the development of~~  
631 ~~the TDM has also provided insights into hydrological processes in tile-drained landscapes. These~~  
632 ~~are discussed in more detail below.~~

633

#### 634 4.1 *Insights into key control mechanisms of tile flow for catchment-scale simulations*

635 The model suggests that tile flow may not be accurately predicted exclusively based on the  
636 ~~matric potential~~water table depth and soil saturated hydraulic conductivity as suggested by the  
637 steady-state flow assumptions of the Hooghoudt's equation (Hooghoudt, 1940). ~~These Our~~ results  
638 indicate two additional controls: (1) the amount of drainable soil water in the soil, which has also  
639 been identified in some field studies (*e.g.*, Skaggs et al., 1978; Moriasi et al., 2013) and (2)  
640 fluctuations in the groundwater table (GWRD) are ~~equally~~ important to account for in  
641 catchment-scale simulations. However, the relationship between drainable water and tile flow  
642 rates is non-linear, as demonstrated in Fig. 7a. This is because the residence time for  
643 groundwater seepage and evapotranspiration increases when the hydraulic tile carrying capacity  
644 is exceeded. Comparatively, the effect of soil drainable water,  $\varphi_s$  (see also Fig. 7a) on tile flow is  
645 small because the capillary fringe and associated drainable soil water control the amount of water  
646 that can effectively flow to the tile.

647

648 The verification of the model also indicated that the slopes of the rising and falling limbs of tile  
649 flow hydrographs and WT were very sensitive to (1) the ratio between K and drainable soil  
650 water; and (2) the net outflow in the soil through tile flow and groundwater level fluctuations  
651 (GWRD). This is supported by previous studies showing rapid responses of tile flow to  
652 precipitation events (Gentry et al., 2007; Smith et al., 2015) and others that have related rapid  
653 responses in tile discharge to antecedent moisture conditions (Macrae et al., 2007; Vidon and  
654 Cuadra, 2010; Lam et al., 2016a; Macrae et al., 2019), which can be affected by the development  
655 of a capillary fringe and its ~~holding capacity~~non-drainable water.  
656

657 Results show that large fluctuations in WT (or SSS) and tile flow during the cold season, when  
658 the water table tends to be above the tile, are primarily triggered by the development of a  
659 capillary fringe that reduces the amount of drainable soil water. Model sensitivity tests showed  
660 that a small amount of drainable soil water produces steeper rising and falling responses (and  
661 with larger fluctuation amplitudes) in both the water table (saturated storage) and the tile flow.  
662 Indeed, this pattern can be observed by exploring differences in tile drain responses in clay loam  
663 soils with larger field capacities (and correspondingly smaller drainable water) and smaller  
664 hydraulic conductivity which are more likely to experience pronounced oscillations (*e.g.*, steeper  
665 rising and falling response curves) compared to tile drain responses of sandy soil, which is  
666 characterized by reduced capillary forces, lower field capacities (but correspondingly larger  
667 drainable water) and higher hydraulic conductivity. Notably, both model and observations of  
668 ~~WT/SSS~~ (as a proxy for soil moisture) reveal a bimodal (*i.e.*, two peaks) frequency distribution  
669 when examined in relation to the tile depth and capillary fringe thickness (Fig. 8 and 9,  
670 respectively). The two peaks (*i.e.* most frequently observed WT or SSS conditions) correspond

671 with the (1) depth of the tile pipe (0.75 m), which demonstrates the efficacy of the tile at rapidly  
672 removing excess soil water, and the (2) the capillary fringe thickness (for the depths of 1.0 and  
673 1.4 m, Figs. g, h, i and j) beyond which the amount of drainable water above the water ~~level~~table  
674 significantly increases.

675

676 These findings align well with studies such as Lam et al. (2016a) that recorded soil moisture near  
677 saturation after tile flow had ceased, suggesting the development of a capillary fringe. Combined  
678 experimental and modeling works, such as in Moriasi et al. (2013) and Logsdon et al. (2010),  
679 also discuss the impact of drainable soil water (“drainable porosity” or “specific water yield”) on  
680 tile flow and note that the drainable water is, in turn, dependent on the soil type, soil-water  
681 dynamic and water table depth. However, these studies did not explore the dynamic nature of the  
682 capillary fringe and its thickness relative to the soil column above in determining the transient  
683 amount of drainage soil water that will impact the WT distribution and tile flow differently over  
684 time (*Conditions 1 to 3*, see Fig. 2). Herein, while a capillary fringe with a fixed thickness that is  
685 generally related to the soil properties was assumed, its vertical positioning was simulated  
686 dynamically, which allowed determining the drainable soil water based on the evolution of  
687 pressure head corresponding to field capacity. Thus, the development of the TDM has provided  
688 a step forward in the modeling of tile drainage and suggests that in loam soils such as those at the  
689 study site, the effects of a capillary fringe on tile flow should be included. Soil moisture (soil  
690 unsaturated storage) measurements from the study site by Van Esbroeck et al., (2017) between  
691 November 2011 and May 2014 from depths of 10, 30, and 50 cm (using EC-5 Soil Moisture  
692 Smart Sensor) showed that almost 90% of the gravitational soil moisture drains out with 0.5 to  
693 2.5 h. ~~It reveals~~suggests that the water table and capillary fringe can reach to an equilibrium

694 conditionation within one hour at this field site, enabling us to and we were allowed to use a  
695 steady state equation (Hooghoudt, 1940) to predict the dynamic behavior of the water table  
696 fluctuations.

697  
698 *4.2 Importance of capturing seasonal patterns in groundwater to improve tile flow*  
699 *predictions*

700 The GWRD changed dramatically between seasons affecting soil moisture (both saturated and  
701 unsaturated storage of the soil) and tile flow patterns. Both observations and model results show  
702 that low precipitation and higher evapotranspiration rates tend to produce little tile flow during  
703 the growing season. These seasonal patterns in precipitation and evapotranspiration are  
704 accompanied by a reduction in soil moisture (both unsaturated storage and saturated storage )  
705 that leads to a substantial storage capacity in fields. Even following moderate and high-intensity  
706 storms during the growing season, rapid soil moisture increases are observed (both saturated and  
707 unsaturated soil storage); however, tile flow rarely develops, suggesting that the soil is able to  
708 hold the water (Lam et al., 2016a; Van Esbroeck et al., 2016). In contrast, tile flow is often  
709 observed during the cold season, even during smaller rainfall-runoff and snowmelt events  
710 because of reduced soil storage but also a seasonal increase in GWRD (Lam et al., 2016a;  
711 Macrae et al., 2007, 2019; Van Esbroeck et al., 2016). This concurs with several studies  
712 throughout the Great Lakes and St. Lawrence region that have reported stronger tile responses  
713 during the non-growing season, with the summer months often showing little to no tile flow  
714 (Lam et al., 2016a, 2016b; Jamieson et al., 2003; Macrae et al., 2007; Hirt et al., 2011; King et  
715 al., 2016; Van Esbroeck et al., 2016; Plach et al., 2019).

716

717 These results (the controlling effect of soil drainable water and groundwater level fluctuations on  
718 tile flow) suggest that while soil moisture (both [saturatedSSS](#) and unsaturated storage) is largely  
719 controlled by tile flow rather than GWRD in the cold season, this reverses in the growing season  
720 (*i.e.*, soil moisture controls tile flow), with soil moisture (both [saturatedSSS](#) and unsaturated  
721 storage) being also impacted by evapotranspiration. The controlling effect of groundwater  
722 fluctuations in the growing season has also been studied by Hansen et al., (2019). The model  
723 indicated that the rapid drops in observed ~~in~~ WT during the growing season could not be  
724 explained by evapotranspiration alone as well as the crop root depths, thus pointing to the role of  
725 GWRD. Johnsen et al. (1995) and Akis (2016) also showed that the effect of groundwater  
726 accretion was more effective on tile flows than surface runoff. Also, Vaughan et al. (1999) found  
727 that tile drain flows in their study site in San Joaquin Valley of California were better explained  
728 and related to nonlocal groundwater appearance than to local variations in irrigation amount,  
729 evapotranspiration, variation in water storage or tile drain blockage. ~~So~~Thus, it was  
730 figureddetermined out that other in addition to than soil saturated hydraulic conductivity and soil  
731 thickness, the seasonal groundwater fluctuations and capillary fringe drainable water are other  
732 important controlling factors on tile flow rates.

733

## 734 **5. Conclusion**

735 A new tile drain module within the modular Cold Regions Hydrological Modelling ([CRHM](#))  
736 platform has been created and tested at the field scale to support the management of agricultural  
737 basins with seasonal snow covers. The model was tested and validated for a small working farm  
738 in southern Ontario, Canada, and presents a step forward in the dynamic simulation of tile flow  
739 and its effects on the hydrological cycle in cold climates. Observations and model results showed

740 that the dynamic prediction of tile flow and soil moisture at catchment scales needs to account  
741 for (1) the amount of drainable soil water that can be affected by the development of a capillary  
742 fringe and (2) fluctuations in the groundwater water table, in addition to the typical (3) ~~matric~~  
743 potential water table elevation above the tile pipe and (4) the soil saturated hydraulic conductivity  
744 considered by the steady-state flow Hooghoudt's equation.

745  
746 The groundwater table and matric potential changed dramatically between seasons, affecting  
747 patterns of soil moisture and tile flow. Observations and model results showed that low  
748 precipitation and higher evapotranspiration rates caused minimal tile flows during the crop-  
749 growing season. Conversely, tile flow was often observed during the cold season, even during  
750 small rainfall-runoff and snowmelt events, due to a seasonal increase in the groundwater table  
751 and ~~soil-saturated~~soil-saturated storage.

752  
753 Model sensitivity tests showed that the capillary fringe strongly affected the amount of drainable  
754 soil water flowing into the tile. Tile flow increased with drainable water, but the relationship is  
755 highly non-linear likely because, as the tile carrying capacity is exceeded more frequently, there  
756 is more opportunity time for groundwater seepage and evapotranspiration. Finally, observations  
757 and model results reveal a bimodal ~~soil-saturated~~soil-saturated storage response in the presence  
758 of tiles, which is controlled by the relative positioning of the capillary fringe in relation to the  
759 soil surface and the depth of tile drains below the soil surface. Capturing these dynamics is a  
760 critical advance enabling the accurate prediction of the swift hydrological changes caused by the  
761 presence of tiles in models.



762 The TDM was developed as a first approximation from a single field site. Given this limitation, it  
763 is not yet widely applicable across multiple field sites ~~yet~~. However, the development of this  
764 module ~~has provided~~ valuable-critical insights into ~~the-its~~ potential and performance for hourly  
765 time-step simulations, as well as the importance of regional groundwater table fluctuations and  
766 simplifying the capillary fringe parameters within models in some landscape types. Future work  
767 will include building on the model and adapting it for different soil textures, such as those in clay  
768 loam soils, where -preferential flow can have a strong impact on ~~soil-saturated~~ soil-saturated  
769 storage and tile flow. Also, explicit representation of unsaturated flow will be needed to enable  
770 the use of the model regions where groundwater is disconnected from surface water, as  
771 commonly happens in arid and semi-arid regions. Subsequent steps include also the development  
772 integration of the new TDM model with CRHM's ~~of~~ water quality modules.

773

#### 774 **Code/Data availability**

775 The tile flow and soil water table data are not publicly available and will be provided upon  
776 request to the data owner, Merrin Macrae. TDM code is not completely implemented in the main  
777 version of the Cold Regions Hydrological Model platform and is provided only upon request to  
778 the corresponding author.

779

#### 780 **Author contribution**

781 MK and DC developed the model code and performed the simulations. MM prepared the data  
782 and supported the field work. MK, DC and MM prepared the manuscript with contributions from  
783 JP and RP. All authors edited the manuscript.

784

785 **Competing interests**

786 The contact author has declared that none of the authors has any competing interests.

787

788 **Acknowledgements**

789 Funding for this project was provided by the Canada First Excellence Research Fund's Global  
790 Water Futures programme through its Agricultural Water Futures project. Funding for the  
791 collection of the field data was provided by the Ontario Ministry of Agriculture, Food and Rural  
792 Affairs. The support of the Biogeochemistry Lab at the University of Waterloo for the collection  
793 of field data and of Tom Brown and Xing Fang of the Centre for Hydrology at the University of  
794 Saskatchewan for CRHM development and updates is gratefully acknowledged. The Maitland  
795 Valley Conservation Authority is thanked for providing some precipitation, rainfall, and  
796 temperature data.

797

798 **References**

799 Akis R.: Simulation of Tile Drain Flows in an Alluvial Clayey Soil Using HYDRUS 1D,  
800 American-Eurasian J. Agric. & Environ. Sci., 16 (4), 801-813,  
801 <https://doi.org/10.5829/idosi.aejaes.2016.16.4.12906>, 2016.

802

803 Arheimer, B., Nilsson, J., and Lindstrom, G.: Experimenting with Coupled Hydro-Ecological  
804 Models to Explore Measure Plans and Water Quality Goals in a Semi-Enclosed Swedish Bay,  
805 Water, 7(7), 3906-3924, <https://doi.org/10.3390/w7073906>, 2015.

806

807 Arnold, J. G., Srinivasan, R., Muttiah, R. S., and Williams, J. R.: Large area hydrologic  
808 modeling and assessment part I: model development, J. Am. Water. Resour. Assoc., 34, 73-89,  
809 <https://doi.org/10.1111/j.1752-1688.1998.tb05961.x>, 1998.  
810

811 Badr, A. W.: Physical properties of some North Carolina Organic Soils and the effect of land  
812 development on these properties, M.S. Thesis, Department of Biological and Agricultural  
813 Engineering, North Carolina State University, Raleigh, NC. 67 p., 1978.  
814

815 Blear, W. (2<sup>nd</sup> Edition): Soil and Environmental Chemistry, Academic Press, eBook ISBN:  
816 9780128041956, 2017.  
817

818 Bouwer, H. and van Schilfhaarde, J.: Simplified method of predicting the fall of water table in  
819 drained land, Trans. ASAE. 6(4), 288-291, 296, 1963.  
820

821 Brockley, R. P.: The effect of nutrient and moisture on soil nutrient availability, nutrient uptake,  
822 tissue nutrient concentration, and growth of Douglas-Fir seedlings, Master Thesis, The  
823 University of British Columbia, 1976.  
824

825 Broughton, R. and Jutras, P.: Farm Drainage. In the Canadian Encyclopedia,  
826 <https://www.thecanadianencyclopedia.ca/en/article/farm-drainage/>, last access: 14 February  
827 2019.  
828

829 Coelho, B. B., Murray, R., Lapen, D., Topp, E., and Bruin, A.: Phosphorus and sediment loading  
830 to surface waters from liquid swine manure application under different drainage and tillage  
831 practices, *Agric. Water Manag.*, 104, 51-61, <https://doi.org/10.1016/j.agwat.2011.10.020>, 2012.  
832

833 Cordeiro, M. R. C. and Ranjan, R. S.: Corn yield response to drainage and subirrigation in the  
834 Canadian Prairies, *Trans. ASABE*. 55(5), 1771-1780, <https://doi.org/10.13031/2013.42369>,  
835 2012.

836

837 Cordeiro, M. R. C., Wilson, H. F., Vanrobaeys, J., Pomeroy, J. W., Fang, X., and The Red-  
838 Assiniboine Project Biophysical Modeling Team: Simulating cold-region hydrology in an  
839 intensively drained agricultural watershed in Manitoba, Canada, using the Cold Region  
840 Hydrological Model, *Hydrol. Earth Syst. Sci.*, 21, 3483-3506, [https://doi.org/10.5194/hess-21-](https://doi.org/10.5194/hess-21-3483-2017)  
841 [3483-2017](https://doi.org/10.5194/hess-21-3483-2017), 2017.

842

843 Correll, D.: The role of phosphorus in the eutrophication of receiving waters: a review, *J.*  
844 *Environ. Qual.*, 27, 261-266, <https://doi.org/10.2134/jeq1998.00472425002700020004x>, 1998.  
845

846 Costa, D., Klenk, K., Knoben, W., Ireson, A., Spiteri, R., Clark, M.: A multi-chemistry  
847 modelling framework to enable flexible and reproducible water quality simulations in existing  
848 hydro-models: 1. The OpenWQ concept and the water quality modelling lab. ESS Open Archive.  
849 <https://essopenarchive.org/doi/full/10.22541/essoar.168718167.75677635/v1>, -2023  
850

851 Costa, D., Klenk, K., ~~Wouter Johannes Maria~~Knoben, W.J.M.,-et al Ireson, A., Spiteri, R.J.,  
852 Clark, M.P.:- A multi-chemistry modelling framework to enable flexible and reproducible water  
853 quality simulations in existing hydro-models: 2. The OpenWQ-SUMMA and OpenWQ-CRHM  
854 model implementations and testing. ESS Open Archive.

855 [DOI:10.22541/essoar.168652285.59958331/v1](https://doi.org/10.22541/essoar.168652285.59958331/v1), 2023.

856

857 Costa, D., Sutter, D., Shepherd, A., Jarvie, H., Wilson, H., Elliott, J., Liu, J., and Macrae, M.:  
858 Impact of climate change on catchment nutrient dynamics: insights from around the  
859 world. Environmental Reviews. **31**(1): 4-25. <https://doi.org/10.1139/er-2021-0109>, 2022

860

861 Costa, D., Baulch, H., Elliott, J., Pomeroy, J., and Wheeler, H.: Modelling nutrient dynamics in  
862 cold agricultural catchments: A review, Environ. Model. Softw., 124, 104586,  
863 <https://doi.org/10.1016/j.envsoft.2019.104586>, 2020a.

864

865 Costa, D., Shook, K., Spence, C., Elliott, J., Baulch, H., Wilson, H., and Pomeroy, J.: Predicting  
866 variable contributing areas, hydrological connectivity, and solute transport pathways for a  
867 Canadian Prairie basin, Water Resour. Res., 56, 1-23, <https://doi.org/10.1029/2020WR02798>,  
868 2020b.

869

870 Costa, D., Burlando, P., Liong, S.-Y.: Coupling spatially distributed river and groundwater  
871 transport models to investigate contaminant dynamics at river corridor scales. Environmental  
872 Modelling & Software, 86, 91–110. <https://doi.org/10.1016/j.envsoft.2016.09.009>, 2016

873

874 Costa, D., Pomeroy, J. W., Brown, T., Baulch, H., Elliott, J., and Macrae, M.: Advances in the  
875 simulation of nutrient dynamics in cold climate agricultural basins: Developing new nitrogen and  
876 phosphorus modules for the Cold Regions Hydrological Modelling Platform, *J. Hydrol.*, 603, 1-  
877 17, <https://doi.org/10.1016/j.jhydrol.2021.126901>, 2021.

878

879 Clark, M. P., Nijssen, B., Lundquist, J. D., Kavetski, D., Rupp, D. E., Woods, R. A., Freer, J. E.,  
880 Gutmann, E. D., Wood, A. W., Brekke, L. D., Arnold, J. R., Gochis, D. J., & Rasmussen, R. M.  
881 (2015). A unified approach for process-based hydrologic modeling: 1. Modeling concept. *Water*  
882 *Resources Research*, 51(4), 2498–2514. <https://doi.org/https://doi.org/10.1002/2015WR017198>

883

884 Clark, M. P., Nijssen, B., Lundquist, J. D., Kavetski, D., Rupp, D. E., Woods, R. A., Freer, J. E.,  
885 Gutmann, E. D., Wood, A. W., Gochis, D. J., Rasmussen, R. M., Tarboton, D. G., Mahat, V.,  
886 Flerchinger, G. N., & Marks, D. G. (2015). A unified approach for process-based hydrologic  
887 modeling: 2. Model implementation and case studies. *Water Resources Research*, 51(4), 2515–  
888 2542. <https://doi.org/https://doi.org/10.1002/2015WR017200>

889

890 De Ridder, N. A., Takes, C. A. P., van Someren, C. L., Bos, M. G., Messemaeckers van de  
891 Graaff, R. H., Bokkers, A. H. J., Stransky, J., Wiersma-Roche, M. F. L., and Beekman, T.:  
892 *Drainage Principles and Applications*. International Institute for Lan Reclamation and  
893 Improvement, P.O. Box 45 Wageningen The Netherlands, 1974.

894

895 Du, B., Arnold, J. G., Saleh, A., and Jaynes, D. B.: Development and application of SWAT to  
896 landscapes with tiles and potholes, Trans. ASAE, 48, 1121-1133,  
897 <https://doi.org/10.13031/2013.18522>, 2005.

898

899 Du, B., Saleh, A., Jaynes, D. B., and Arnold, J. G.: Evaluation of SWAT in simulating nitrate  
900 nitrogen and atrazine fates in a watershed with tiles and potholes, Trans. ASABE, 49, 949-959,  
901 <https://doi.org/10.13031/2013.21746>, 2006.

902

903 ECCC, Canadian Climate Normals 1981-2010 Station Data,  
904 [https://climate.weather.gc.ca/climate\\_normals/results\\_1981\\_2010\\_e.html?searchType=stnProx&txtRadius=25&selCity=&selPark=&optProxType=custom&txtCentralLatDeg=43&txtCentralLatMin=41&txtCentralLatSec=55&txtCentralLongDeg=81&txtCentralLongMin=28&txtCentralLongSec=47&txtLatDecDeg=&txtLongDecDeg=&stnID=4545&dispBack=0](https://climate.weather.gc.ca/climate_normals/results_1981_2010_e.html?searchType=stnProx&txtRadius=25&selCity=&selPark=&optProxType=custom&txtCentralLatDeg=43&txtCentralLatMin=41&txtCentralLatSec=55&txtCentralLongDeg=81&txtCentralLongMin=28&txtCentralLongSec=47&txtLatDecDeg=&txtLongDecDeg=&stnID=4545&dispBack=0), last access: 5  
907 February 2020.

908

909

910 Eckersten, H., Jansson, P. -E., and Johnsson, H. (2<sup>nd</sup> edition): SOILN model-user's manual,  
911 Division of Agricultural Hydrotechnics Communications 94:4, Department of soil Sciences,  
912 Swedish University of Agricultural Sciences, 58pp, Uppsala, 1994.

913

914 Environment Canada, Canadian Climate Normals 1981-2010 Station Data,  
915 [https://climate.weather.gc.ca/climate\\_data/daily\\_data\\_e.html?hlyRange=%7C&dlyRange=1966-06-01%7C2021-06-14&mlyRange=1966-01-01%7C2006-12-01&StationID=4603&Prov=ON&urlExtension=\\_e.html&searchType=stnName&optLimit=year](https://climate.weather.gc.ca/climate_data/daily_data_e.html?hlyRange=%7C&dlyRange=1966-06-01%7C2021-06-14&mlyRange=1966-01-01%7C2006-12-01&StationID=4603&Prov=ON&urlExtension=_e.html&searchType=stnName&optLimit=year)

918 [Range&StartYear=1840&EndYear=2022&selRowPerPage=25&Line=0&searchMethod=contain](#)  
919 [s&Month=6&Day=4&txtStationName=Wroxeter&timeframe=2&Year=2021](#), last access: 10  
920 May 2020.

921

922 Fang, X., Pomeroy, J. W., Westbrook, C. J., Guo, X., Minke, A. G., and Brown, T.: Prediction of  
923 snowmelt derived streamflow in a wetland dominated prairie basin, *Hydrol. Earth Syst. Sci.*, 14,  
924 991-1006, <https://doi.org/10.5194/hess-14-991-2010>, 2010.

925

926 Fang, X., Pomeroy, J. W., Ellis, C. R., MacDonald, M. K., DeBeer, C. M., and Brown, T.: Multi-  
927 variable evaluation of hydrological model predictions for a headwater basin in the Canadian  
928 Rocky Mountains, *Hydrol. Earth Syst. Sci.*, 17, 1635-1659, [https://doi.org/10.5194/hess-17-](https://doi.org/10.5194/hess-17-1635-2013)  
929 [1635-2013](https://doi.org/10.5194/hess-17-1635-2013), 2013.

930

931 Filippelli, G. M.: The global phosphorus cycle, *Rev. Mineral. and Geochem.*, 48, 391-425,  
932 <https://doi.org/10.2138/rmg.2002.48.10>, 2002.

933

934 Frey, S. K., Hwang, H. T., Park, Y. J., Hussain, S. I., Gottschall, N., Edwards, M., and Lapen, D.  
935 R.: Dual permeability modeling of tile drain management influences on hydrologic and nutrient  
936 transport characteristics in macroporous soil, *J. Hydrol.*, 535, 392-406,  
937 <http://dx.doi.org/10.1016/j.jhydrol.2016.01.073>, 2016.

938



939 Gentry, L. E., David, M. B., Royer, T. V., Mitchell, C. A., and Starks, K.: Phosphorus transport  
940 pathways to streams in tile-drained agricultural watersheds, *J. Environ. Quality.*, 36, 408-415,  
941 <https://doi.org/10.2134/jeq2006.0098>, 2007.

942

943 Garcia-Gutierrez, C., Pachepsky, Y., and Martin, M. A.: Technical note: Saturated hydraulic  
944 conductivity and textural heterogeneity of soils, *Hydrol. Earth Syst. Sci.*, 22, 3923-3932,  
945 <https://doi.org/10.5194/hess-22-3923-2018>, 2018.

946

947 Green, C. H., Tomer, M. D., Di Luzio, M., and Arnold, J. G.: Hydrologic evaluation of the Soil  
948 and Water Assessment Tool for large tile-drained watershed in Iowa, *Trans. ASABE.*, 49, 413-  
949 422, <https://doi.org/10.13031/2013.20415>, 2006.

950

951 Hansen, A. L., Jakobsen, R., Refsgaard, J. C., Hojberg, A. L., Iversen, B. V., and Kjaergaard, C.:  
952 Groundwater dynamics and effect of tile drainage on water flow across the redox interface in a  
953 Danish Weichsel till area, *Advances in Water Resources*, 123, 23-39,  
954 <https://doi.org/10.1016/j.advwatres.2018.10.022>, 2019.

955

956 Hirt, U., Wetzig, A., Amatya, M. D., and Matranga, M.: Impact of seasonality on artificial  
957 drainage discharge under temperate climate conditions, *Int. Rev. Hydrobiol.*, 96, 561-577,  
958 <https://doi.org/10.1002/iroh.201111274>, 2011.

959

960 Hooghoudt, S. B.: Bijdrage tot de kennis van enige natuurkundige grootheden van de grand.  
961 Verslagen van Landbouwkundige Onderzoekingen, 46(7), 515-707, the Hague, The Netherlands  
962 (in Dutch), 1940.

963

964 ICID: World Drained Area-2018. International Commission on Irrigation and Drainage.  
965 <http://www.icid.org/world-drained-area.pdf> , last access: 14 February 2019.

966

967 Jamieson, A., Madramootoo, C. A., and Enright, P.: Phosphorus losses in surface and subsurface  
968 runoff from a snowmelt event on an agricultural field in Quebec, Can. Biosyst. Eng., 45, 11-17,  
969 2003.

970

971 Jarvie, H. P., Johnson, L. T., Sharpley, A. N., Smith, D. R., Baker, D. B., Bruulsema, T. W., and  
972 Confesor, R.: Increased Soluble Phosphorus Loads to Lake Erie: Unintended Consequences of  
973 Conservation Practices?, J. Environ. Qual., 46, 123-132,  
974 <https://doi.org/10.2134/jeq2016.07.0248>, 2017.

975

976 Javani-Jouni, H., Liaghat, A., Hassanoghli, A., and Henk, R.: Managing controlled drainage in  
977 irrigated farmers' fields: A case study in the Moghan Plain, Iran, Agric. Water Manag., 208, 393-  
978 405, <https://doi.org/10.1016/j.agwat.2018.06.037>, 2018.

979

980 Johnsen, K. E., Liu, H. H., Dane, J. H., Ahuja, L. R., and Workman, S. R.: Simulating  
981 Fluctuating Water Tables and Tile Drainage with a Modified Root Zone Water Quality Model

982 and a New Model WAFLOWM, Transactions of the ASAE, 38 (1), 75-83,  
983 <https://doi.org/10.10031/2013.27814>, 1995.

984

985 Kiesel, J., Fohrer, N., Schmalz, B., and White, M. J.: Incorporating landscape depressions and  
986 tile drainages of a northern German lowland catchment into a semi-distributed model, Hydrol.  
987 Process., 24, 1472-1486, <https://doi.org/10.1002/hyp.7607>, 2010.

988

989 King, K. W., Williams, M. R., Macrae, M. L., Fausey, N. R., Frankenberger, J., Smith, D. R.,  
990 Kleinman, P. A. J., and Brown, L. C.: Phosphorus transport in agricultural subsurface drainage:  
991 A review, J. Environ. Qual., 44(2), 467-485, <https://doi.org/10.2134/jeq2014.04.0163>, 2015.

992

993 King, K. W., Williams, M. R., and Fausey, N. R.: Effect of crop type and season on nutrient  
994 leaching to tile drainage under a corn-soybean rotation, J. Soil and Water Conserv., 71, 56-68,  
995 <https://doi.org/10.2489/jswc.71.1.56>, 2016.

996

997 Kirkham, D.: Theory of land drainage, in, Drainage of Agricultural Lands. Agronomy  
998 Monograph, No. 7, American Society of Agronomy, Madison, Wisconsin, 1957.

999

1000 Kladivko, E. J., Grochulska, J., Turco, R. F., Van Scoyoc, G. E., and Eigel, J. D.: Pesticide and  
1001 nitrate transport into subsurface tile drains of different spacings, J. Environ. Qual., 28, 997-1004,  
1002 <https://doi.org/10.2134/jeq1999.00472425002800030033x>, 1999.

1003

1004 Klaiber, L. B., Kramer, S. R., and Young, E. O.: Impacts of Tile Drainage on Phosphorus Losses  
1005 from Edge-of-field Plots in the Lake Champlain Basin of New York, *Water*, 12, 328,  
1006 <https://doi.org/10.3390/w12020328>, 2020.

1007

1008 Kock, S., Bauwe, A., and Lennartz, B.: Application of SWAT Model for a Tile-Drained Lowland  
1009 Catchment in North-Eastern Germany on Subbasin Scale, *Water Resour. Manage.*, 27, 791-805,  
1010 <https://doi.org/10.1007/s11269-012-0215-x>, 2013.

1011

1012 Kokulan, V.: Environmental and Economic Consequences of Tile Drainage Systems in Canada,  
1013 The Canadian Agri-Food Policy Institute (CAPI), 2019.

1014

1015 Kokulan, V., Macrae, M. L., Ali, G. A., and Lobb, D. A.: Hydroclimatic controls on runoff  
1016 activation in a artificially drained, near-level vertisolic clay landscape in a Prairie climate, *Hyrol.*  
1017 *Process.*, 33, 602-615, <https://doi.org/10.1002/hyp.13347>, 2019a.

1018

1019 Lam, W. V., Macrae, M. L., English, M. C., O'Halloran, I. P., Plach, J. M., and Wang, Y.:  
1020 Seasonal and event-based drives of runoff and phosphorus export through agricultural tile drains  
1021 under sandy loam soil in a cool temperate region, *Hydrol. Process.*, 30, 2644-2656,  
1022 <https://doi.org/10.1002/hyp.10871>, 2016a.

1023

1024 Lam, W. V., Macrae, M. L., English, M. C., O'Halloran, I., and Wang, Y.: Effects of tillage  
1025 practices on phosphorus transport in tile drain effluent in sandy loam agricultural soils in

1026 Ontario, Canada, *J. Great Lakes Res.*, 42(6), 1260-1270,  
1027 <https://dx.doi.org/10.1016/j.jglr.2015.12.015>, 2016b.  
1028  
1029 Larsbo, M., and Jarvis, N.: MACRO 5.0. A model of water flow and solute transport in  
1030 microporous soil, Technical description. Swedish University of Agricultural Sciences, Division  
1031 of Environmental Physics, Emergo 2003:6 Report, ISSN 1651-7210, ISBN 91-576-6592-3,  
1032 2003.  
1033  
1034 Lindstrom, G., Pers, C., Rosberg, J., Stromqvist, J., and Arheimer, B.: Development and testing  
1035 of the HYPE (Hydrological Predictions for the Environment) water quality model for different  
1036 scales, *Hydrol. Res.*, 41(3-4), 295-319, <https://doi.org/10.2166/nh.2010.007>, 2010.  
1037  
1038 Logsdon, S. D., Schilling, K. E., Hernandez-Ramirez, G., Prueger, J. H., Hatfield, J. L., and  
1039 Sauer, T. J.: Field estimation of specific yield in a central Iowa crop field, *Hydrol. Process.*, 24,  
1040 1369-1377, <https://doi.org/10.1002/hyp.7600>, 2010.  
1041  
1042 Macrae, M. L., English, M. C., Schiff, S. L., and Stone, M. L.: Intra-annual variability in the  
1043 contribution of tile drains to basin discharge and phosphorus export in a first order agricultural  
1044 catchment, *Agric. Water Manag.*, 92, 171-182, <https://doi.org/10.1016/j.agwat.2007.05.015>,  
1045 2007.  
1046  
1047 Macrae, M. L., Ali, G. A., King, K. W., Plach, J. M., Puer, W. T., Williams, M., Morison, M.  
1048 Q., and Tang, W.: Evaluating Hydrologic Response in Tile-Drained Landscapes: Implications for

1049 Phosphorus Transport, *J. Environ. Qual.*, 48(5), 1347-1355,  
1050 <https://doi.org/10.2134/jeq2019.02.0060>, 2019.  
1051  
1052 Malzone, J. M., Lowry, C. S., and Ward, A. S.: Response of the hyporheic zone to transient  
1053 groundwater fluctuations on the annual and storm event time scales, *Water Resour. Res.*, 52,  
1054 5301-5321, <https://doi.org/10.1002/2015WR018056>, 2016.  
1055  
1056 Mizukami, N., Clark, M. P., Sampson, K., Nijssen, B., Mao, Y., McMillan, H., Viger, R. J.,  
1057 Markstrom, S. L., Hay, L. E., Woods, R., Arnold, J. R., & Brekke, L. D. (2016). mizuRoute  
1058 version 1: A river network routing tool for a continental domain water resources applications.  
1059 *Geoscientific Model Development*, 9, 2223–2238. <https://doi.org/10.5194/gmd-9-2223-2016>  
1060 Moriasi, D. N., Arnold, J. G., Van Liew, M. W., Bingner, R. L., Harmel, R. D., and Veith, T. L.:  
1061 Model Evaluation Guidelines for Systematic Quantification of Accuracy in Watershed  
1062 Simulations, *Trans. ASABE*, 50(3), 885-900, <https://doi.org/10.13031/2013.23153>, 2007.  
1063  
1064 Moriasi, D. N., Gowda, P. H., Arnold, J. G., Mulla, D. J., Ale, S., Steiner, J. L., and Tomer, M.  
1065 D.: Evaluation of the Hooghoudt and Kirkham Tile Drain Equations in the Soil and Water  
1066 Assessment Tool to Simulate Tile Flow and Nitrate-Nitrogen, *J. Environ. Qual.*, 42, 1699-1710,  
1067 <https://doi.org/10.2134/jeq2013.01.0018>, 2013.  
1068  
1069 Plach, J. M., Macrae, M. L., Ali, G. A., Brunke, R. R., English, M. C., Ferguson, G., Lam, W.  
1070 V., Lozier, T. M., McKague, K., O'Halloran, I. P., Opolko, G., and Van Esbroeck, C. J.: Supply  
1071 and Transport Limitations on Phosphorus Losses from Agricultural Fields in the Lower Great

1072 Lakes Region, Canada, *J. Environ. Qual.*, 47, 96-105, <https://doi.org/10.2134/jeq2017.06.0234>,  
1073 2018a.  
1074  
1075 Plach, J. M., Macrae, M. L., Williams, M. R., Lee, B. D., and King, K. W.: Dominant glacial  
1076 landforms of the lower Great Lakes region exhibit different soil phosphorus chemistry and  
1077 potential risk for phosphorus loss, *J. Great Lakes Res.*, 44, 1057-1067,  
1078 <https://doi.org/10/1016/j.jglr.2018.07.005>, 2018b.  
1079  
1080 Plach, J., Puer, W., Macrae, M., Kompanizare, M., McKague, K., Carlow, R., and Brunke, R.:  
1081 Agricultural Edge of Field Phosphorus Losses in Ontario, Canada: Importance of the  
1082 Nongrowing Season in Cold Regions, *J. Environ. Qual.*, 48, 813-821,  
1083 <https://doi.org/10.2134/jeq2018.11.0418>, 2019.  
1084  
1085 Puer, W. T., Macrae, M., Buckley, A., and Reid, K.: Contribution of preferential flow to tile  
1086 drainage varies spatially and temporally, *Vadose Zone J.*, 19: e20043,  
1087 <https://doi.org/10.1002/vzj2.20043>, 2020.  
1088  
1089 Pomeroy, J. W., Gray, D. M., Shook, K. R., Toth, B., Essery, R. L. H., Pietroniro, A., and  
1090 Hedstrom, N. R.: An evaluation of snow accumulation and ablation processes for land surface  
1091 modelling, *Hydrol. Process.*, 12, 2339-2367, [https://doi.org/10.1002/\(SICI\)1099-  
1092 1085\(199812\)12:15](https://doi.org/10.1002/(SICI)1099-1085(199812)12:15), 1998.  
1093

1094 Pomeroy, J. W., Gray, D. M., Brown, T., Hedstrom, N. R., Quinton, W. L., Granger, R. J., and  
1095 Carey, S. K.: The cold regions hydrological model: a platform for basing process representation  
1096 and model structure on physical evidence, *Hydrol. Process.*, 21, 2650-2667,  
1097 <https://doi.org/10.1002/hyp.6787>, 2007.

1098

1099 Pomeroy, J. W., Fang, X., Shook, K., and Whitfield, P. H.: Predicting in Ungauged Basins Using  
1100 Physical Principles Obtained Using the Deductive, Inductive, and Abductive Reasoning  
1101 Approach, [https://research-](https://research-groups.usask.ca/hydrology/documents/pubs/papers/pomeroy_et_al_2003_3.pdf)  
1102 [groups.usask.ca/hydrology/documents/pubs/papers/pomeroy\\_et\\_al\\_2003\\_3.pdf](https://research-groups.usask.ca/hydrology/documents/pubs/papers/pomeroy_et_al_2003_3.pdf) , 2013.

1103

1104 Pomeroy, J. W., Fang, X., and Marks, D. G.: The cold rain-on-snow event of June 2013 in the  
1105 Canadian Rockies - characteristics and diagnosis, *Hydrol. Process.*, 30, 2899-2914,  
1106 <https://doi.org/10.1002/hyp.10905>, 2016.

1107

1108 Pomeroy, J. W., Brown, T., Fang, X., Shook, K. R., Pradhananga, D., Armstrong, R., Harder, P.,  
1109 Marsh, C., Costa, D., Krogh, S. A., Aubry-Wake, C., Annand, H., Lawford, P., He, Z.,  
1110 Kompanizare, M., and Lopez Moreno, J. I.: The cold regions hydrological modelling platform  
1111 for hydrological diagnosis and prediction based on process understanding, *J. of Hydrol.*, 615 (A),  
1112 128711, <https://doi.org/10.1016/j.jhydrol.2022.128711>, 2022.

1113

1114 Qi, P., Zhang, G., Xu, Y. J., Wang, L., Ding, C., and Cheng, C.: Assessing the Influence of  
1115 Precipitation on Shallow Groundwater Table Response Using Combination of Singular Value



1116 Decomposition and Cross-Wavelet Approaches, *Water*, 10, 598,  
1117 <https://doi.org/10.3390/w10050598>, 2018.  
1118  
1119 Quinton, J. G., Govers, G., van Oost, K., and Bardgett, R.: The impact of agricultural soil erosion  
1120 on biochemical cycling, *Nat. Geosci.*, 3, 311-314, <https://doi.org/10.1038/ngeo838>, 2010.  
1121  
1122 Raats, P. A. C. and Gardner, W. R.: Movement of water in saturated zone near a water table. Ch.  
1123 13 in *Drainage for agriculture*, J. van Schilfgraade, Ed., *Agronomy Monograph*. No. 17,  
1124 American Society of Agronomy, Madison, WI, pp. 331-357, 1974.  
1125  
1126 Radcliffe, D. E., Reid, D. K., Blomback, K., Bolster, C. H., Collick, A. S., Easton, Z. M.,  
1127 Francesconi, W., Fuka, D. R., Johnsson, H., King, K., Larsbo, M., Youssef, M. A., Mulkey, A.  
1128 S., Nelson, N. O., Persson, K., Ramirez-Avila, J. J., Schmieder, F., and Smith, D. R.:  
1129 Applicability of Models to Predict Phosphorus Losses in Drained Fields: A Review, *J. Environ.*  
1130 *Qual.*, 44, 614-628, <https://doi.org/10.2134/jeq2014.05.0220>, 2015.  
1131  
1132 Rahman, M. M., Lin, Z., Jia, X., Steele, D. D., and DeSutter, T. M.: Impact of subsurface  
1133 drainage on streamflows in Red River of the North basin, *J. Hydrol.*, 511, 474-483,  
1134 <https://doi.org/10.1016/j.jhydrol.2014.01.070>, 2014.  
1135  
1136 Refsgaard, J. C. and Storm, B.: MIKE SHE. In: Singh VP (ed) *Computer models of watershed*  
1137 *hydrology*, Highlands Ranch, Water Research Pub, Colorado, 1995.  
1138

1139 Richards L. A.: Capillary conduction of liquids through porous medium, *Physics*, 1 (5): 318-333,  
1140 Bibcode:1931Physi...1..318R. <https://doi.org/10.1063/1.1745010>, 1931.  
1141  
1142 Rozemeijer, J. C., Visser, A., Borren, W., Winegram, M., van der Velde, Y., Klein, J., and  
1143 Broers, H. P.: High-frequency monitoring of water fluxes and nutrient loads to assess the effects  
1144 of controlled drainage on water storage and nutrient transport, *Hydrol. Earth Syst. Sci.*, 20, 347-  
1145 358, <https://doi.org/10.5194/hess-20-347-2016>, 2016.  
1146  
1147 Rust, W., Holman, I., Bloomfield, J. Cuthbert, M., and Corstanje, R.: Understanding the potential  
1148 of climate teleconnections to project future groundwater drought, *Hydrol. Earth Syst. Sci.*, 23,  
1149 3233-3245, <https://doi.org/10.5194/hess-23-3233-2019>, 2019.  
1150  
1151 Ruttenberg, K.: The global phosphorus cycle. In *Biochemistry*, Vol. 8, treatise on geochemistry,  
1152 Schlesinger W (ed) (eds. H. Holland and K. Turekian). Elsevier-Pergamon: Oxford; 585-643,  
1153 2005.  
1154  
1155 Searcy, J. and Hardison, C. H.: Double –Mass Curves. *Manual of Hydrology: Part 1, General*  
1156 *Surface-Water Techniques*, Geological Survey Water-Supply Paper 1541-B, 1960.  
1157  
1158 Schindler, D. W.: Recent advances in the understanding and management of eutrophication,  
1159 *Limnol. Oceanogr.*, 51, 356-363, [https://doi.org/10.4319/lo.2006.51.1\\_part\\_2.0356](https://doi.org/10.4319/lo.2006.51.1_part_2.0356), 2006.  
1160

1161 Sharpley, A. N., Hedley, M. J., Sibbesen, E., Hillbricht-Ilkowska, A., House, W. A., and  
1162 Ryszkowski, L.: Phosphorus transfer from terrestrial to aquatic ecosystems, In Phosphorus in the  
1163 global environment, Tiessen H (ed), Scientific Committee on Problems of the Environment  
1164 (SCOPE). John Wiley & SonsLtd.: Chichester; 171-199, 1995.

1165

1166 Simunek J., van Genuchten M. Th., and Sejna M.: The HYDRUS Software Package for  
1167 Simulating Two- and Three-Dimensional Movement of Water, Heat and Multiple Solutes in  
1168 Variably-Saturated Media, Technical Manual, Version 2.0, PC Progress, Prague, Czech  
1169 Republic, pp. 258, 2011.

1170

1171 Skaggs, R. W.: A water management model for shallow water table soils, University of North  
1172 Carolina, Water Resource Research Institute, Technical Report 134, 1978.

1173

1174 Skaggs, R. W.: Combination surface-subsurface drainage systems for humid regions. J. Irrig.  
1175 Drain. Div., ASCE. 106(IR4), 265-283, 1980a.

1176

1177 Skaggs, R. W.: Drainmod Reference Report, Methods for Design and Evaluation of Drainage-  
1178 Water Management Systems for Soils with High Water Tables, U.S. Department of Agriculture,  
1179 Soil Conservation Service, North Carolina State University, Raleigh, North Carolina, 1980b.

1180

1181 Skaggs, R. W., Wells, L. G., and Ghate, S. R.: Predicted and measured drainable porosities for  
1182 field soils, Trans. ASAE, 21(3), 522-528, [https://uknowledge.uky.edu/bae\\_facpub/199](https://uknowledge.uky.edu/bae_facpub/199), 1978.

1183

1184 Skaggs, R. W., Youssef, M. A., and Chescheir, G. M.: DRAINMOD: Model Use, Calibration,  
1185 and Validation, Trans. ASABE, 55(4), 1509-1522, <https://doi.org/10.13031/2013.42259>, 2012.  
1186

1187 Smedema, L. K., Vlotman, W. F., and Rycroft, D.: Modern land Drainage. Planning, design and  
1188 management of agricultural drainage systems, London: Taylor & Francis.  
1189 <https://doi.org/10.1201/9781003>, 2004.  
1190

1191 Smith, D. R., King, K. W., Johnson, L., Francesconi, W., Richards, P., Baker, D., and Sharpley,  
1192 A. N.: Surface runoff and tile drainage transport of phosphorus in the Midwestern United States,  
1193 J. Environ. Qual., 44, 495-502, <https://doi.org/10.2134/jeq2014.04.0176>, 2015.  
1194

1195 Tomer, M. D., Meek, D. W., Jaynes, D. B., and Hatfield, J. L.: Evaluation of nitrate nitrogen  
1196 fluxes from a tile-drained watershed in Central Iowa, J. Environ. Qual., 32, 642-653,  
1197 <https://doi.org/10.2134/jeq2003.6420>, 2003.  
1198

1199 Twarakavi, N. K. C., Sakai, M., and Simunek, J.: An objective analysis of the dynamic nature of  
1200 field capacity, Water Resour. Res., 45, W10410, <https://doi.org/10.1029/2009WR007944>, 2009.  
1201

1202 Van Esbroeck, C. J., Macrae, M. L., Brunke, R. I., and McKague, K.: Annual and seasonal  
1203 phosphorus export in surface runoff and tile drainage from agricultural fields with cold temperate  
1204 climates, J. Great Lakes Res., 42(6), 1271-1280, <https://doi.org/10.1016/j.jglr.2015.12.014>, 2016.  
1205

1206 Van Esbroeck, C. J., Macrae, M. L., Brunke, R. R., and McKague, K.: Surface and subsurface  
1207 phosphorus export from agricultural fields during peak flow events over the nongrowing season  
1208 in regions with cool, temperate climates, *Journal of Soil and Water Conservation*, 72(1), 65-76,  
1209 <https://doi:10.2489/jswc.72.1.65> , 2017.

1210  
1211 Van Schilfgaarde, J.: Nonsteady flow to drains, In *Drainage for Agriculture*, J. van Schilfgaarde,  
1212 ed. American Society of Agronomy, Madison, WI. PP 245-270, 1974.

1213  
1214 Vaughan, P. J., Suarez, D. L., Simunek, J., Corwin, D. L., and Rhoades, J. D.: Role of  
1215 Groundwater Flow in Tile Drain Discharge, *J. Environ. Qual.*, 28, 403-410,  
1216 <https://doi.org/10.2134/jeq1999.00472425002800020006x>, 1999.

1217  
1218 Vidon, P. and Cuadra, P. E.: Impact of precipitation characteristics on soil hydrology in tile  
1219 drained landscapes, *Hydrol. Process.*, 24, 1821-1833, <https://doi.org/10.1002/hyp.7627>, 2010.

1220  
1221 Vivekananthan, K.: Environmental and Economic Consequences of Tile Drainage Systems in  
1222 Canada, The Canadian Agri-Food Policy Institute, [www.capi-icpa.ca](http://www.capi-icpa.ca), 2019.

1223  
1224 Vivekananthan, K., Macrae, M., Lobb, D. A., and Ali, G. A.: Contribution of overland and tile  
1225 flow to runoff and nutrient losses from vertisols in Manitoba, Canada, *J. Environ. Qual.*, 48(4),  
1226 959-965, <https://doi.org/10.2134/jeq2019.03.0103>, 2019.

1227

1228 Waichler, S. R. and Wigmosta, M. S.: Development of Hourly Meteorological Values from  
1229 Daily Data and Significance to Hydrological Modeling at H. J. Andrews Experimental Forest,  
1230 Am. Meteorol. Soc., 4, 251-263, [https://doi.org/10.1175/1525-  
1231 7541\(2003\)4<251:DOHMFV>2.0.CO;2](https://doi.org/10.1175/1525-7541(2003)4<251:DOHMFV>2.0.CO;2), 2003.

1232

1233 Williams, M. R., King, K. W., and Fausey, N. R.: Drainage water management effects on tile  
1234 discharge and water quality, Agric. Water Manag., 148, 43-51,  
1235 <http://dx.doi.org/10.1016/j.agwat.2014.09.017>, 2015.

1236

1237 Williams, M. R., King, K. W., Ford, W., Buda, A. R., and Kennedy, C. D.: Effect of tillage on  
1238 macropore flow and phosphorus transport to tile drains, Water Resour. Res., 52, 2868-2882,  
1239 <https://doi.org/10.1002/2015WR017650>, 2016.

1240

1241 Williams, M. R., Livingston, S. J., Heathman, G. C., and McAfee, S. J.: Thresholds for run-off  
1242 generation in a drained closed depression, Hydrol. Process., 1-14,  
1243 <https://doi.org/10.1002/hyp.13477>, 2019.

1244

1245 Youngs, E. G.: Effect of the Capillary fringe on Steady-State Water Tables in drained Lands, J.  
1246 Irrig. Drain. Eng., 138(9), 809-814, [https://doi.org/10.1061/\(ASCE\)IR.1943-4774.0000467](https://doi.org/10.1061/(ASCE)IR.1943-4774.0000467),  
1247 2012.

1248

1249

1250 **Appendix A**

1251 Table A1. Instrument names and descriptions

<b>Instrument name</b>	<b>Description</b>
Hach Flo-tote and FL900 logger	Flow velocity and water level measurement
U20, Onset Ltd.	Barometrically-corrected pressure transducer
Temperature Smart Sensor S-THB-M002	Air temperature measurement
Wind Smart Sensor S-WSET-M002	Wind speed measurement
(Silicon Pyranometer)-S-LIB-M003	Solar radiation sensor
Tipping bucketrain gauge, 0.2 mm Rainfall Smart Sensor – SRGB-M002	Rainfall measurement
RH Smart Sensor(S-THB-M002)	Relative Humidity measurement

1252

1253

1254

1255 **Appendix B**

1256 Table B1. Parameter names and their symbols in CRHM platform

<b>Parameter symbol</b>	<b>Parameter name</b>
Tair	Air temperature
Wspeed	Wind speed
RH	Relative Humidity
Qsi	Incoming solar irradiance
R	Rainfall
WQ_soil	Water Quality soil module
WT	Water table elevation above the semipermeable layer

SSS	Soil saturated storage or the saturated part of the soil moisture
soil_moist	Soil moisture
Porosity_soil	Soil porosity
AL	Above layer
BL	Below layer
GWRD	Groundwater level fluctuations, groundwater recharge and discharge

1257

1258

1259

1260 **Appendix C**

1261

1262 ~~Here, it was shown~~We show how ~~we assess~~seasonal factors ( $f_{y,i}$ ) is assessed for different years  
 1263 ~~in this study~~. Equation (4) can be written as:

1264

$$1265 \quad G_{y,i} = G \times f_{y,i} \quad (C1)$$

1266

1267 For each year ( $y$ ),  $f_{y,i}$  for the first ( $f_{y,1}$ ) and second ( $f_{y,2}$ ) part of the sine function ( $G$ ) were  
 1268 assessed individually. It should be note that in first and second part of the sine function for each  
 1269 year, where  $G$  is larger than zero ( $-G \geq 0$ ) and smaller than zero ( $G < 0$ ), respectively.  $G$  can be  
 1270 defined for the two parts, were defined as:

1271

$$1272 \quad \begin{cases} \text{if } G \geq 0 \text{ [ } i = 1 \text{ ] then } f_{y,1} = x \\ \text{if } G < 0 \text{ [ } i = 2 \text{ ] then } f_{y,2} = y \end{cases} \quad (C-2)$$



1273

1274

$G$  is the sine function representing the annual fluctuations in water table (WT/SSS) or it can be

1275

simply defined as the percolation rate (in  $\text{mm hr}^{-1}$ ) of soil water to groundwater through lower

1276

semi-permeable layer. So, for  $n$  years there are  $n \times 2 f_{y,i}$  values. The default values for  $f_{y,i}$  are 1

1277

and the default values can be changed for each year and for first and second parts in each year

1278

independently. Calculated  $G_{y,i}$  in each time step add or subtracted to or from the total soil

1279

moisture depend on ~~the~~ its sign. The  $f_{y,i}$  values for the sine function parameters are presented in

1280

Fig. C1. The verified sine function time series along with time series of temperature,

1281

precipitation and calculated evapotranspiration are shown in Fig. C1. In this figure it is obvious

1282

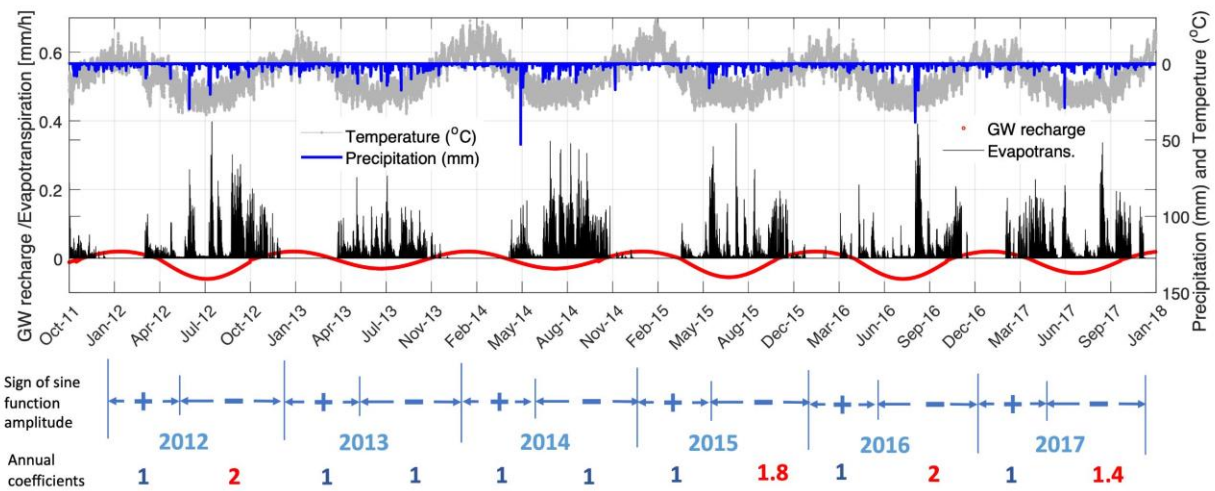
that in years 2012 and 2015 to 2017 the warm season amplitudes are larger. The ET values are

1283

happened more in the warm seasons (growing seasons). Also, ~~it can be seen that~~ the seasonal

1284

oscillation in sine function is very similar to the temperature general oscillations.



1285

1286

Figure C1. Time series of the adjustable sine function along with the time series of calculated evapotranspiration, temperature

1287

and precipitation during the study period from Oct 2011 to Sept 2018.

1288

1289

1290

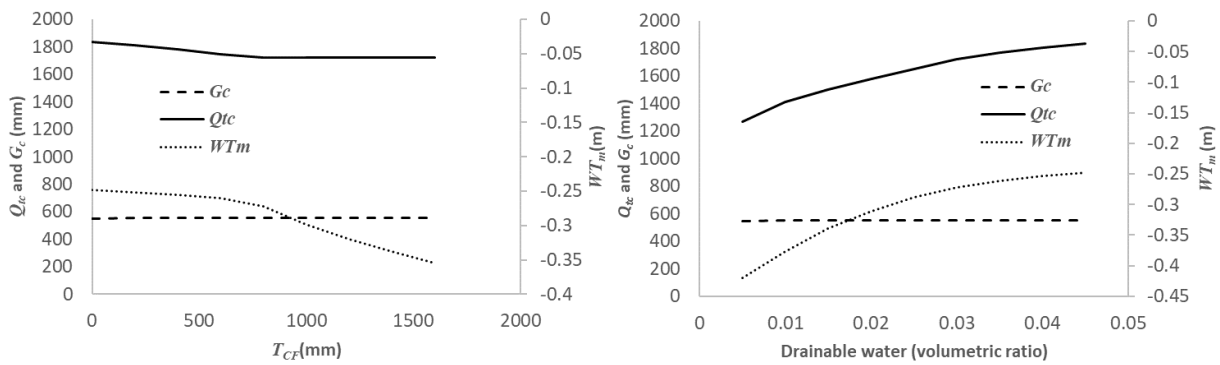
## Appendix D

1291 ~~A~~We conducted sensitivity analysis was conducted for the cumulative tile flow ( $Q_{tc}$ ), mean soil  
 1292 water table elevation ( $WT_m$ ) and cumulative outflow rate from the ~~soil's bottom~~ semi-permeable  
 1293 layer at the bottom of the soil to groundwater ( $G_c$ ) (see section 2.4.5, Eq. 4) with respect to six  
 1294 module parameters. Additionally, ~~we proposed~~ an approach for assessing model parameters at a  
 1295 new sites, potentially lacking water table elevation and tile flow observations is proposed.

1296

1297 **D.1 Sensitivity analysis**

1298 In this section, ~~we examined~~ the sensitivity of  $Q_{tc}$ ,  $WT_m$  and  $G_c$  to six distinct module  
 1299 parameters, namely capillary fringe thickness ( $T_{CF}$ ), capillary fringe drainable water ( $\varphi_c$ ), soil  
 1300 saturated hydraulic conductivity ( $K$ ), soil thickness ( $T_{SL}$ ), sine function amplitude ( $A$ ) and sine  
 1301 function ( $B$ ) ~~was examined~~.  $Q_{tc}$ ,  $G_c$  and  $WT_m$  were computed over the entire simulation period,  
 1302 expressed in units of mm, mm and m, respectively. Figures D-1a to f illustrate these sensitivities,  
 1303 with each parameter's impact discussed in dedicated sections.

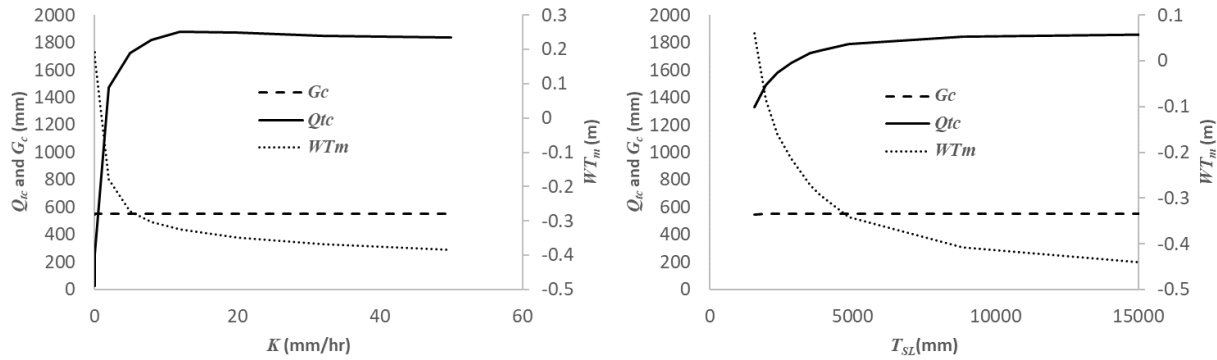


1304

a)

b)

1305

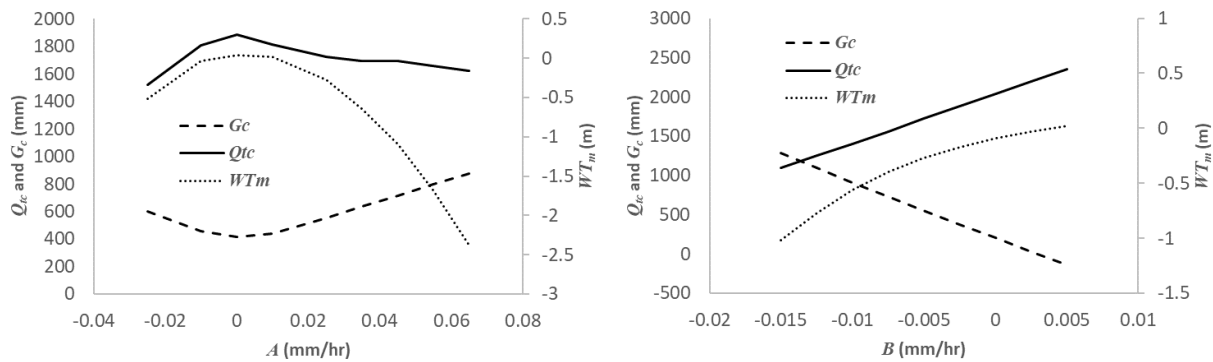


1306

1307

c)

d)



1308

1309

e)

f)

Figure D-1 Sensitivity of cumulative tile flow,  $Q_{tc}$ , cumulative soil to groundwater percolation rate,  $G_c$ , and mean soil water table elevation,  $WT_m$ , to capillary fringe thickness,  $T_{CF}$  (a) capillary fringe drainable water,  $\phi_c$  (b), soil hydraulic conductivity,  $K$  (c), soil thickness,  $T_{SL}$  (d), sine function amplitude,  $A$  (e) and sine function intercept,  $B$  (f).

1313

### D.1.1 Sensitivity to capillary fringe thickness

To gauge sensitivity to capillary fringe thickness  $T_{CF}$ , flow rates and the  $WT_m$  were analyzed for  $T_{CF}$  ranging 0 to 1600 mm. Figure D-1a indicates that as  $T_{CF}$  increases, both cumulative tile flow ( $Q_{tc}$ ) and mean soil water table ( $WT_m$ ) decline. The  $WT_m$  drop is sharper for  $T_{CF}$  beyond 900 mm. Beyond this thickness,  $Q_{tc}$  stabilizes at a minimal value. A negative  $WT_m$  indicates its position below the tile pipe.  $G_c$  remains consistent despite  $T_{CF}$  variations.

1320

1321 D.1.2 Sensitivity to capillary fringe drainable water

1322 With rising  $\varphi_c$  both  $Q_{tc}$  and  $WT_m$  surge (Figure D-1b). As  $\varphi_c$  ascends from 0.005 to 0.45,  $Q_{tc}$   
1323 jumps from 1300 mm to 1900 mm and  $WT_m$  from -0.45 m to -0.25 m (Figure D-1b).  $G_c$  stays  
1324 constant, irrespective of  $\varphi_c$  fluctuations.

1325

1326 D.1.3 Sensitivity to soil hydraulic conductivity

1327 Increasing soil hydraulic conductivity ( $K$ ) from 0 to 10 mm hr<sup>-1</sup> leads to a surge in  $Q_{tc}$  and a drop  
1328 in  $WT_m$  (Figure D-1c). However, adjusting  $K$  from 10 to 50 mm hr<sup>-1</sup> results in leveling off slopes  
1329 for  $Q_{tc}$  and  $WT_m$ , especially when  $K > 20$  mm hr<sup>-1</sup>. Both metrics are acutely responsive to  $K$  when  
1330  $K$  is below 10 mm hr<sup>-1</sup> but become non-responsive beyond 20 mm hr<sup>-1</sup>.  $G_c$ 's response to  $K$   
1331 remains neutral.

1332

1333 D.1.4 Sensitivity to soil thickness

1334 Similar to  $K$ , a rise in  $T_{SL}$  from 1500 mm to 15000 mm causes  $Q_{tc}$  to rise and  $WT_m$  to decline  
1335 (Figure D-1d). The most significant rate of change for both metrics occurs between 1500 to 5000  
1336 mm  $T_{SL}$ . Beyond 5000 mm, changes flatten.  $G_c$  shows no response to  $T_{SL}$  variations.

1337

1338 D.1.5 Sensitivity to sine function amplitude

1339 Increasing the sine function amplitude,  $A$ , from -0.03 to 0 mm hr<sup>-1</sup> pushes both  $Q_{tc}$  and  $WT_m$   
1340 increase and reach to their maximum at  $A=0$  (Figure D-1e). But as  $A$  rises from 0 to 0.06 mm hr<sup>-1</sup>,  
1341 they both decline. In contrast,  $G_c$  descends to its lowest (400 mm) when  $A$  shifts from -0.03 to  
1342 0 and then increases to 900 mm as  $A$  hits 0.063.

1343

1344 D.1.6 Sensitivity to sine function intercept

1345 Both  $Q_{tc}$  and  $WT_m$  ascend with the growth in sine function's intercept,  $B$ . Increasing  $B$  from -  
1346 0.015 to 0.005 mm hr<sup>-1</sup> sees  $G_c$  descend. During this  $B$  increase,  $Q_{tc}$  expands from 1100 to 2400  
1347 mm, while  $G_c$  shrinks from 1400 to 0 mm. It seems the sum of  $Q_{tc}$  and  $G_c$  might be constant.  
1348 This suggests that water either drains through the tile pipe or percolates through the soil bottom.  
1349  $Q_{tc}$ , and  $WT_m$  appear sensitive to all six module parameters, but  $G_c$  only to  $A$  and  $B$ .

1350

1351 **D.2 Module parameter evaluation for new sites**

1352 As discussed in section 2.5, initial values for  $K$ ,  $T_{CF}$  and  $\varphi_c$  can be determined by soil grain-size  
1353 distribution. Parameters less explored in past research for new sites include the sine function's  
1354 amplitude ( $A$ ), intercept ( $B$ ), and time delay ( $D_d$ ).

1355

1356 D.2.1 Evaluating sine function's  $A$  and  $B$

1357 If no percolation exists from the soil's bottom to groundwater and  $G_{y,i}$  is zero, both  $A$  and  $B$   
1358 should be zero. However, if percolation or interactions between soil and groundwater occurs,  $A$   
1359 and  $B$  need calibration assessment. Before this, reasonable initial values and bounds must be set.  
1360 From this study's findings,  $A$  and  $B$  should fall between the mean hourly difference of  
1361 infiltration and observed tile flow rates. For instance, observed hourly rates for infiltration and  
1362 tile flow at our site are 0.07 and 0.03 mm hr<sup>-1</sup>. Thus,  $A$ 's and  $B$ 's initial values should range from  
1363 -0.04 to 0.04 mm hr<sup>-1</sup>. Negative  $A$  and  $B$  values indicate outflow from soil to groundwater and  
1364 vice versa. Initial values were set at 10% of the range limits: -0.004 for  $B$  and 0.004 for  $A$ .  
1365 Eventually,  $B$  and  $A$  were adjusted to -0.005 and 0.025 mm hr<sup>-1</sup>.

1366

1367 *D.2.2 Assessment of sine function's time delay*  
1368 The sine function begins on the first Julian day. If its peak occurs around 91<sup>st</sup> Julian day ( three  
1369 months later), its minimum should be on the 274<sup>th</sup> day. If the peak comes later, say the 111<sup>th</sup> day,  
1370 a 20-day delay is present. This delay should mirror in both function's minima and maxima. In  
1371 this case the minimum would be on day 294. This delay aligns with the soil water table's peak  
1372 annual fluctuations. When no observed fluctuations exist, the delay can be calibrated. A sensible  
1373 initial delay can be ascertained by examining the study site's water table elevations, fitting a sine  
1374 function, and noting the peak's Julian day annually.